

Electronic Supplementary Information for:

Tuning the Emission Properties of Cyclometalated Platinum(II) Complexes by Intramolecular-Electron-Sink/Arylethyngylated Ligands and Its Application For Enhanced Luminescent Oxygen Sensing

Wanhua Wu,^a Wenting Wu,^a Shaomin Ji,^a Huimin Guo,^b Peng Song,^c Keli Han,^c Lina Chi,^a Jingyin Shao^a and Jianzhang Zhao^{a*}

^a State Key Laboratory of Fine Chemicals, School of Chemical Engineering, Dalian University of Technology, 158 Zhongshan Road, Dalian 116012 P. R. China ^b Department of Chemistry, School of Chemical Engineering, Dalian University of Technology, P.O. Box 40, 158 Zhongshan Road, Dalian 116012, P. R. China. ^c Dalian Institute of Chemical Physics, Chinese Academy of Sciences, 457 Zhongshan Road, Dalian 116023, P. R. China.

* zhaojzh@dlut.edu.cn

Index

General information	S2
Synthesis of compound 1 , 3 , 4	S3
Synthesis of compound 5 and 6	S4
Figure S1-S2. ¹ H NMR spectra of 1 , 2	S5
Figure S3-S4. ¹ H NMR spectra of 3 , L-1	S6
Figure S5-S6. ¹³ C NMR and MS spectra of L-1	S7
Figure S7-S8. ¹ H NMR and ¹³ C NMR spectra of Pt-1	S8
Figure S9-S10. MS spectra of Pt-1 and ¹ H NMR of Pt-2	S9
Figure S11-S12. TOCSY and ¹³ CNMR of Pt-2	S10
Figure S13-S14. ¹ H NMR of compound 4 and 5	S11
Figure S15-S16. ¹ H NMR and ¹³ CNMR spectra of L2	S12
Figure S17-S18. MS of L-2 and HNMR spectra of Pt-3	S13
Figure S19-S20. TOCSY and ¹³ C NMR of Pt-2	S14
Figure S21-S22. ¹ H NMR spectra of 6 , L-3	S15
Figure S23-S24. ¹³ C NMR and MS spectra of L-3	S16
Figure S25-S26. ¹ H NMR and ¹³ C NMR spectra of Pt-4	S17
Figure S27-S28. MS of Pt-4 and ¹ H NMR spectra of Pt-5	S18
Figure S29-S30. ¹³ C NMR and MS spectra of Pt-5	S19
Figure S31. Emission of complex Pt-3 in solution under difference atmosphere of Ar, air and oxygen	S20
Figure S32. Emission of Pt-1 and Pt-3 in solution under different concentration of oxygen.....	S20
Figure S33. UV-vis absorption and emission of Pt-1 in solution.....	S21
Figure S34. UV-vis absorption and emission of Pt-2 in solution	S21
Figure S35. Frontier molecular orbital for (ppy)Pt(acac).....	S22
Table S1. Low-lying Electronically Excited States of complex (ppy)Pt(acac).....	S23
Figure S36. Frontier molecular orbital for Pt-1	S24
Table S2. Low-lying Electronically Excited States of complex Pt-1	S25
Figure S37. Frontier molecular orbital for Pt-2	S26
Table S3. Low-lying Electronically Excited States of complex Pt-2	S27
Figure S38. Frontier molecular orbital for Pt-3	S28
Table S4. Low-lying Electronically Excited States of complex Pt-3	S29
Figure S39. Frontier molecular orbital for Pt-4	S30
Table S5. Low-lying Electronically Excited States of complex Pt-4	S31
Figure S40. Frontier molecular orbital for Pt-5	S32
Table S6. Low-lying Electronically Excited States of complex Pt-5	S33
Figure S41. Phosphorescent intensity response of Pt-3 , Pt-4 , Pt-5 to step variations of O ₂ concentration	S34

Figure S42. Fitting of the oxygen sensing property based on the modified Stern-Volmer equation	S35
Table S7 . parameters of O ₂ sensing film.....	S35
Figure S43. CIE color coordinates of the ratiometric oxygen sensing. Pt-2 and Pt-3	S36
Figure S44. HPLC of Pt-1	S37
Figure S45. HPLC of Pt-2	S37

Experimental Section

General

All the chemicals are analytical pure and were used as received. Solvents were dried and distilled for synthesis. NMR spectra were recorded on a 400 MHz Varian Unity Inova NMR spectrophotometer. Mass spectra were recorded with Q-TOF Micro MS spectrometer. UV-Vis absorption spectra were measured with a HP8453 UV-visible spectrophotometer. Fluorescence spectra were recorded on JASCO FP-6500 or a Sanco 970 CRT spectrofluorometer. Fluorescence quantum yields were measured with Ru(bpy)₂(Phen) as the reference ($\Phi = 6.0\%$, in CH₃CN, under deaerated condition). Fluorescence lifetimes were measured on a Horiba Jobin Yvon Fluoro Max-4 (TCSPC) instrument.

All these calculations were performed in Gaussian 09 suit.

Synthesis

n-butyl-4-bromo-1,8-naphthalimide (1)

A solution of n-butylamine (1.28 g, 18 mmol) in ethanol (50 mL) was added dropwise to a mixture of 4-bromo-1,8-naphthalic anhydride (4.0 g, 14 mmol) and ethanol (250 mL) at 60°C under vigorous stirring. The mixture was refluxed for 6 h until the mixture became clear, then cooled to room temperature and filtered to give the crude product as a yellow powder. After recrystallization from anhydrous ethanol, compound 1 was obtained as a white solid. 4.15 g, yield: 89.2%. ^1H NMR (400 MHz, CDCl_3) 8.66 (d, 1H, J = 4.0 Hz), 8.56 (d, 1H, J = 8.4 Hz), 8.41 (d, 1H, J = 6.4 Hz), 8.04 (d, 1H, J = 8.4 Hz), 7.86 (t, 2H, J = 8.4 Hz), 4.17 (t, 2H, J = 8.4 Hz), 1.75–1.68 (m, 2H), 1.50–1.40 (m, 2H), 0.98 (t, 3H, J = 8.4 Hz).

(4-Ethynylphenyl)pyridine (3)

Tetrakis(triphenylphosphine)palladium(0) (106.8 mg, 0.72 mmol) and Cul (274.0 mg, 1.44 mmol) were added to a solution of 2-(4'-Bromophenyl) pyridine (4.06 g, 14.4 mmol) in triethylamine (120 mL) that had been deaerated with argon. Trimethylsilylacetylene (4.1 mL, 28.8 mmol) was added via syringe. The mixture was then heated to 60 °C for 8 h. The solvent was removed under reduced pressure, water was added and the mixture was extracted with dichloromethane (DCM, 4 × 20 mL). The combined organic layer was dried over anhydrous Na_2SO_4 . After removal the solvent the crude product was purified with column chromatography (silica gel, DCM: petroleum ether = 1:4), light yellow oil was abstained. 2.59 g, yield: 72.0 %. Tetrabutylammonium fluoride (1 M in tetrahydrofuran, 36 mL, 36 mmol) was added to a solution of the above trimethylsilane protected intermediate (2.26 g, 8.97 mmol) in tetrahydrofuran (50 mL), and the solution was stirred at room temperature under argon for 3 h. DCM (100 mL) and water (150 mL) were added. The organic layer was separated, and the aqueous layer was extracted with DCM (3 × 15 mL). The combined organic layers were washed with brine (200 mL), dried over anhydrous magnesium sulfate, and filtered, and then the solvent was completely removed. The residue was purified by passing through a silica plug using DCM as eluent to give a yellow solid 3, 1.44 g, 90.0 %. ^1H NMR (400 MHz, CDCl_3): 8.69 (d, 1H, J = 4.7 Hz), 7.97 (d, 2H, J = 8.3 Hz), 7.75–7.69 (m, 2H), 7.60 (d, 2H, J = 8.0 Hz), 7.22 (t, 1H, J = 5.7 Hz), 3.17 (s, 1H).

4-iodobenzonitrile (4)

4-aminobenzonitrile (5.9 g, 0.05 mol) and HCl (18 %, 30 mL) were mixed and cooled to 0–5°C. Solution of NaNO_2 (3.35 g, 51 mmol) in water was added in portions (finish within 1.5 h). The mixture was kept at 0–5°C for 30 min. To the above solution was added 20 mL of acetonitrile. Then solution of KI (8.65 g, 52 mmol) in 15 mL water was added dropwise and bubble evolved (N_2). The mixture was stirred at r.t. overnight. White precipitate obtained. Ethyl acetate (100 mL) was added and the organic layer was washed with saturated NaHSO_3 , saline (2×50 mL), NaHCO_3 (10%) and water. The organic layer was dried over anhydrous MgSO_4 . The solvent was removed under reduced pressure and the crude product was purified by column chromatography (silica gel, petroleum ether/ethyl acetate = 10:1, V/V). Brown solid was obtained, 4.92 g, yield: 43.0 %. ^1H NMR (400 MHz, CDCl_3) 7.86 (d, 2H, J = 8.0 Hz), 7.38 (d, 2H, J = 8.0 Hz).

4-ethynylbenzonitrile (5)

Under nitrogen atmosphere, $\text{Pd}(\text{PPh}_3)_2\text{Cl}_2$ (13.7 mg, 0.02 mmol), Cul (98.0 mg, 0.04 mmol), 4-iodobenzonitrile (614 mg, 2.69 mmol) and triethylamine (5 mL) were mixed together. The mixture was stirred until a clear solution was obtained. Then ethynyl trimethylsilane (527 mg, 5.37 mmol) was added via syringe. The mixture was heated at 45–50 °C for 4 h. Then the reaction mixture was extracted with ethyl acetate (50 mL). The organic layer was

dried over anhydrous Na_2SO_4 . The solvent was removed under reduced pressure to give a pale yellow solid (trimethylsilane protected ethynyl compound). This compound was dissolved in methanol (30 mL) and stirred with K_2CO_3 (1.132 g) for 3 h at r.t. The mixture was filtrated and extracted with diethyl ether. The organic layer was dried and evaporated to give the crude product. The crude product was purified by column chromatography (silica gel, petroleum ether/dichloromethane = 10:1, V/V). Pale yellow solid was obtained, 280.5 mg, yield: 82.2 %. ^1H NMR (400 MHz, CDCl_3) 7.74 (d, 2H, J = 8.0 Hz), 7.58 (d, 2H, J = 8.0 Hz), 3.21 (s, 1H).

1-ethynylnaphthalene (6)

Under argon atmosphere, 1-bromonaphthalene (2.0 g, 9.66 mmol), $\text{Pd}(\text{PPh}_3)_2\text{Cl}_2$ (135.2 mg, 0.193 mmol), PPh_3 (101.2 mg, 0.386 mmol), CuI (73.4 mg, 0.386 mmol) were dissolved in triethylamine (20 mL). After stirring, ethynyltrimethylsilane (1.42 g, 14.5 mmol) was added via syringe. The solution was refluxed for 8 h. The solvent was removed under reduced pressure and the crude product was purified by column chromatography ,silica gel, with hexane as the eluent, light yellow oil was obtained. The above trimethylsilane protected intermediate was dissolved in methanol (30 mL), K_2CO_3 (2.1 g, 15.3 mmol) was added and the mixture was stirred at r.t. for 3 h. The solvent was removed under reduced pressure. Water was added and the mixture was extracted with dichloromethane. The organic layer was dried over anhydrous Na_2SO_4 . After removal the solvent, compound 3 was obtained as light yellow oil. 740 mg, yield: 50.4 %. ^1H NMR (400 MHz, CDCl_3): 8.37 (d, 1H, J = 8.3 Hz), 7.84 (d, 2H, J = 8.0 Hz), 7.74(d, 1H, J = 7.1 Hz), 7.57 (t, 1H, J = 7.3 Hz), 7.51(t, 1H, J = 7.5 Hz), 7.40 (t, 1H, J = 8.1 Hz), 3.46 (s, 1H).

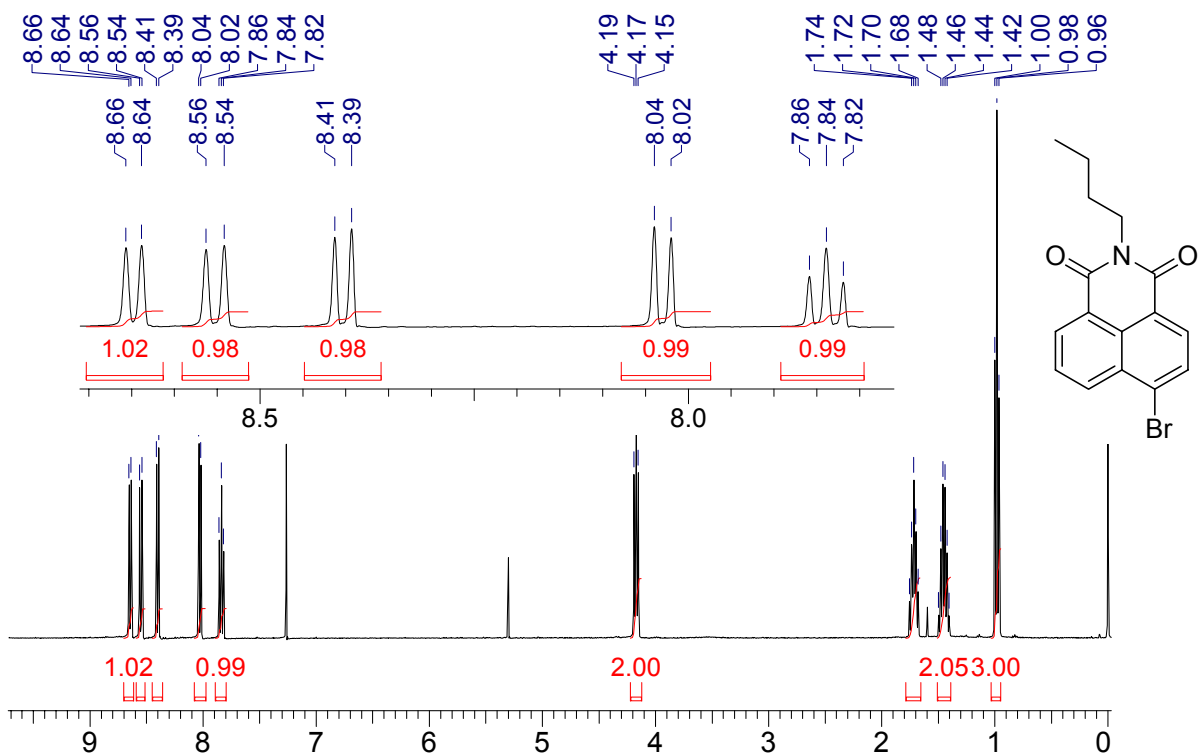


Fig. S1 ^1H NMR of *N*-butyl-4-bromo-1,8-naphthalimide (**1**) (400 MHz, CDCl_3)

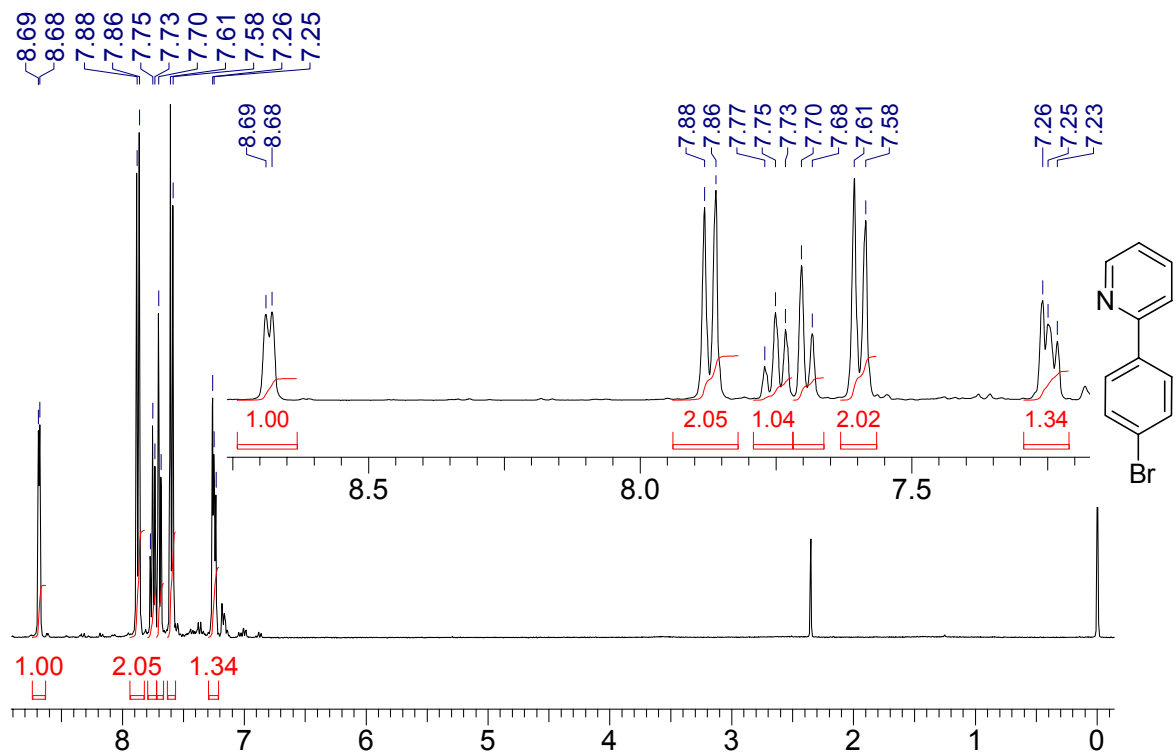


Fig. S2 ^1H NMR of 2-(4-Bromophenyl) pyridine (**2**) (400 MHz, CDCl_3)

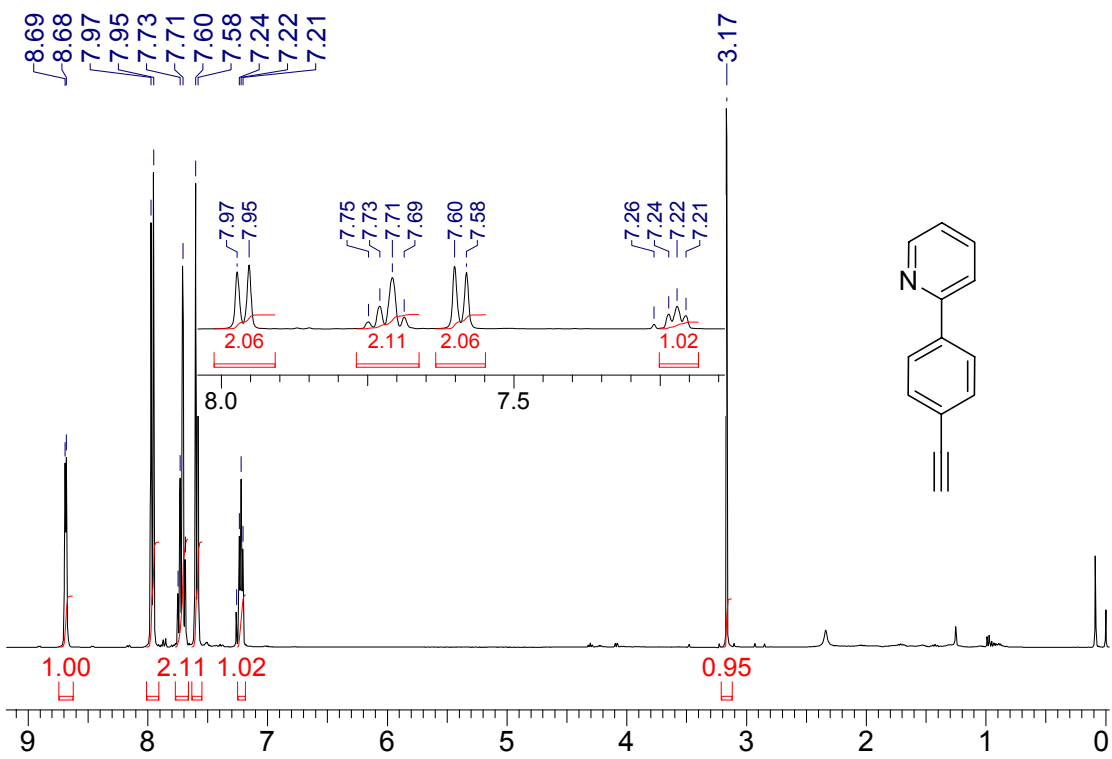


Fig. S3 ^1H NMR of 2-(4-ethynylphenyl)pyridine (**3**) (400 MHz, CDCl_3).

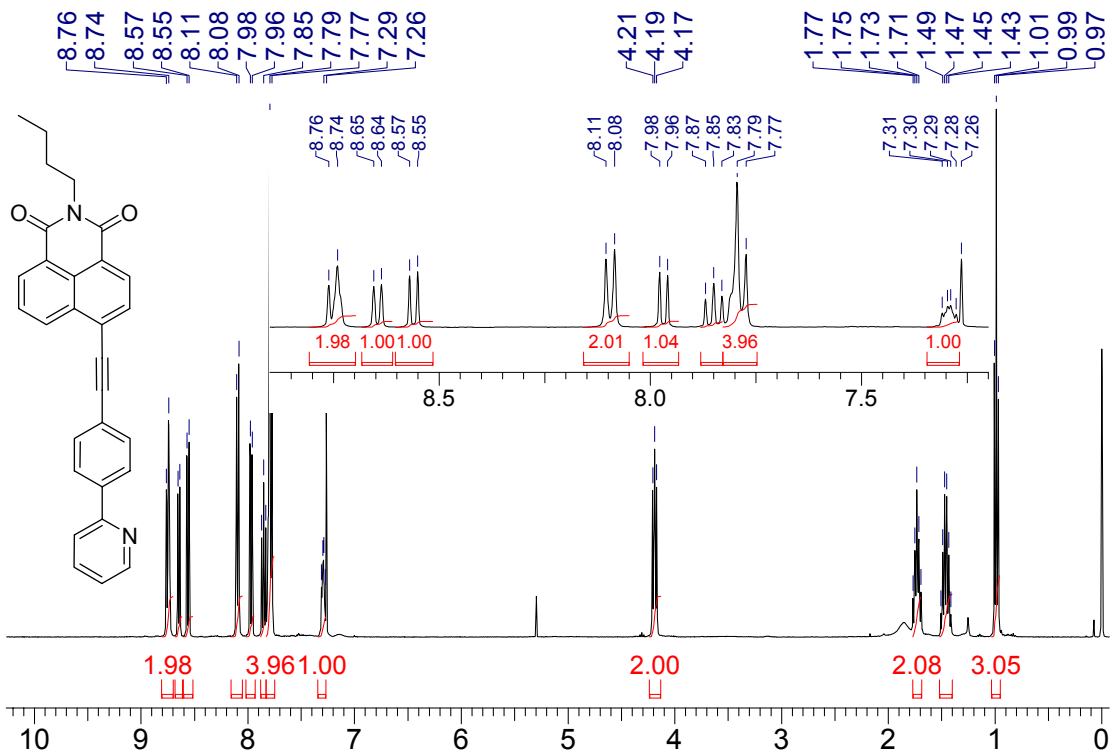


Fig. S4 ^1H NMR of **L1** (400 MHz, CDCl_3).

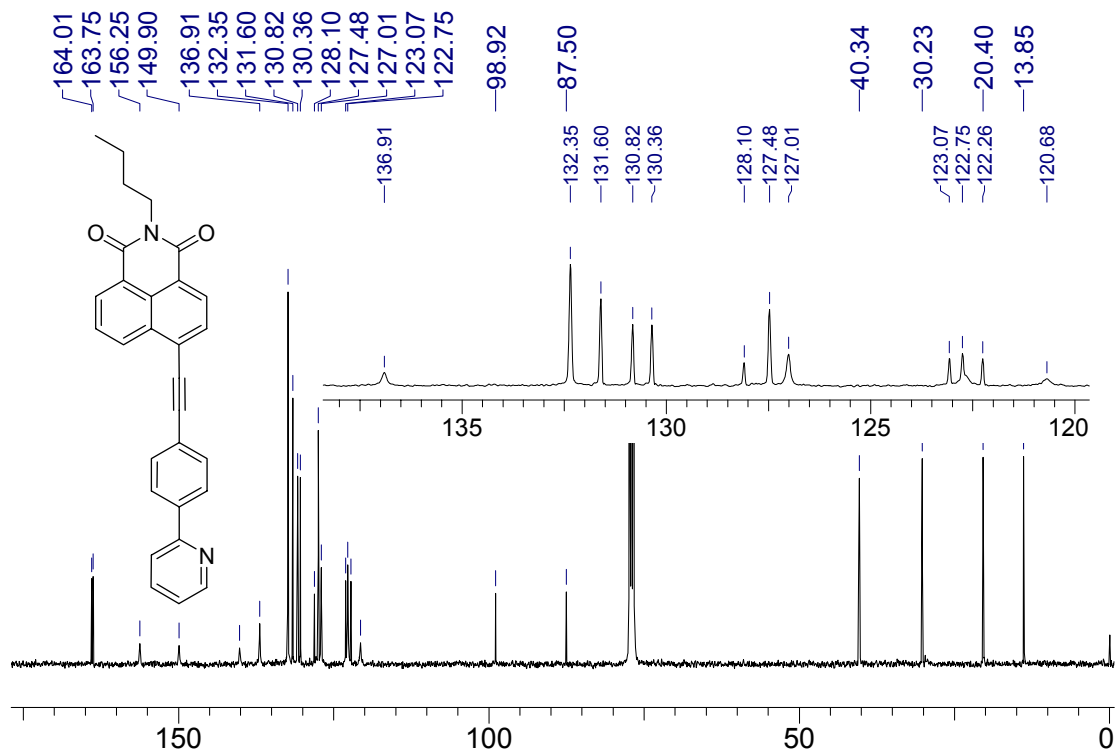


Fig. S5 ¹³C NMR of L1 (100 MHz, CDCl₃).

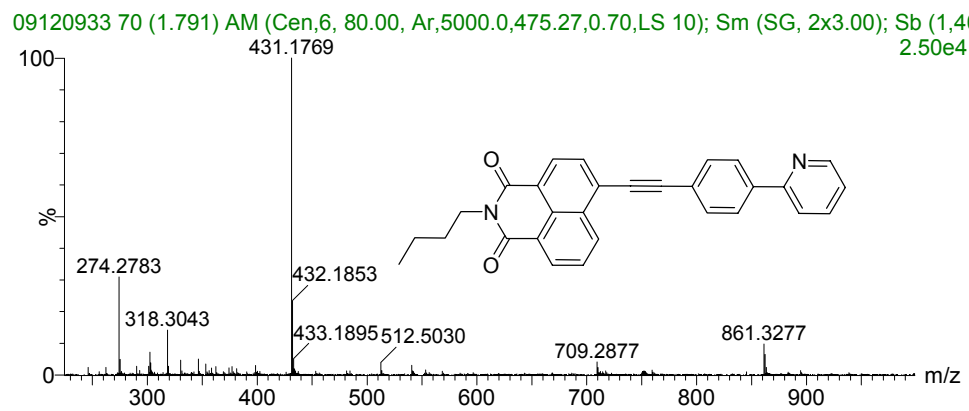


Fig. S6 TOF HRMS ESI of L1.

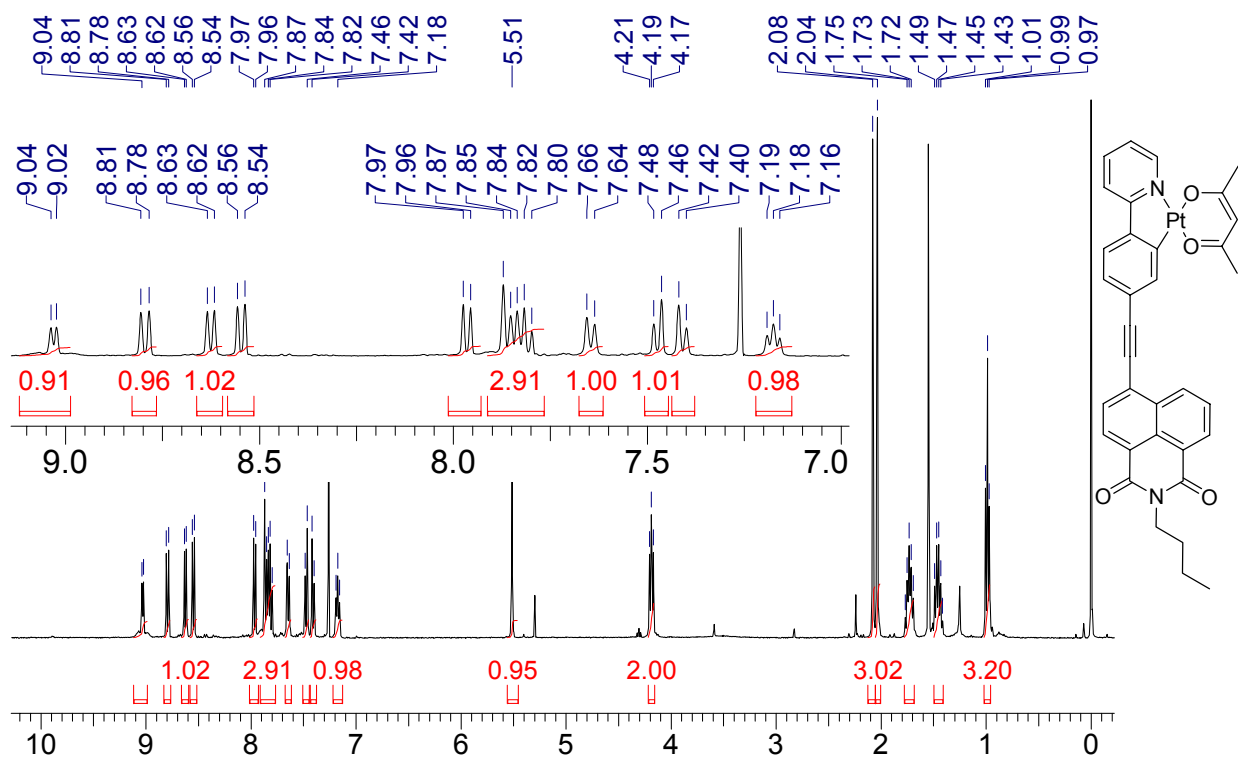


Fig. S7 ^1H NMR of Pt-1 (400 MHz, CDCl_3).

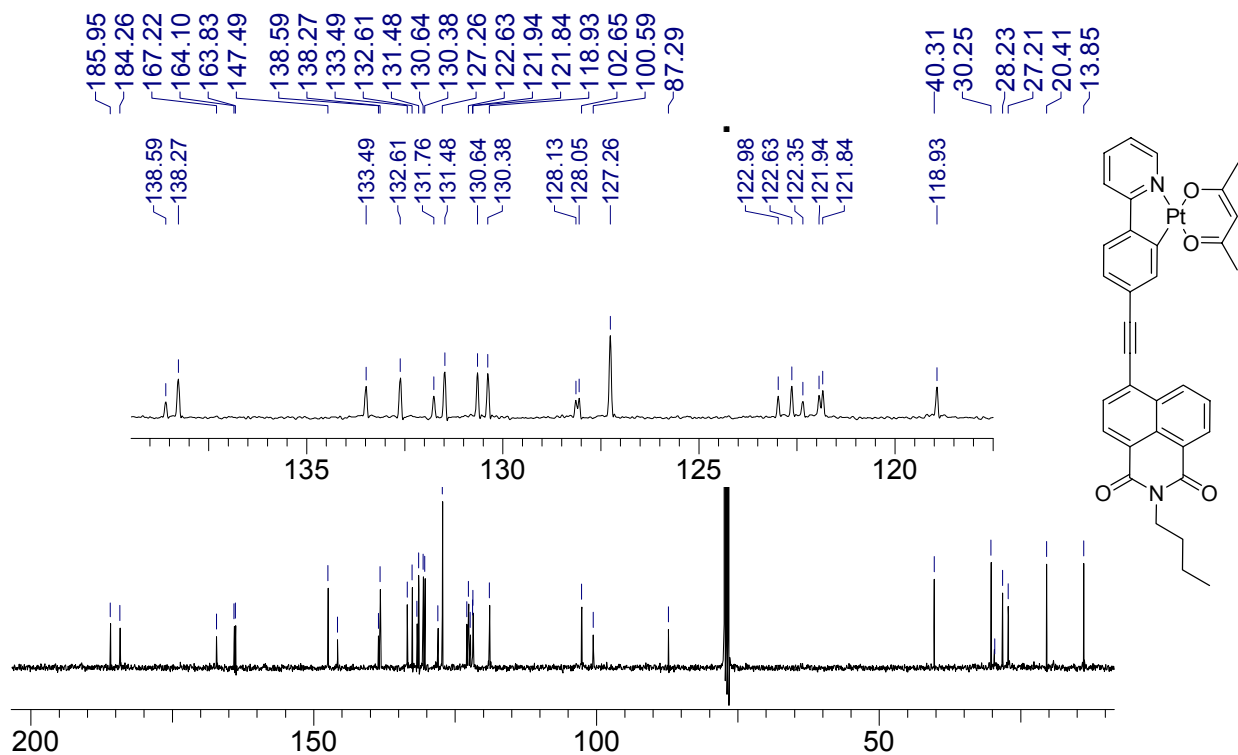


Fig. S8 ^{13}C NMR of Pt-1 (100 MHz, CDCl_3).

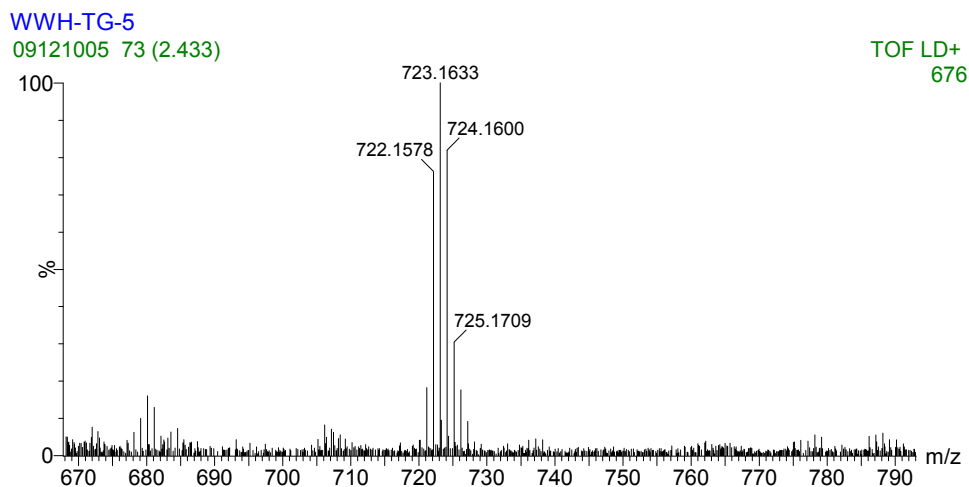


Fig. S9 MALDI-MS of Pt-1.

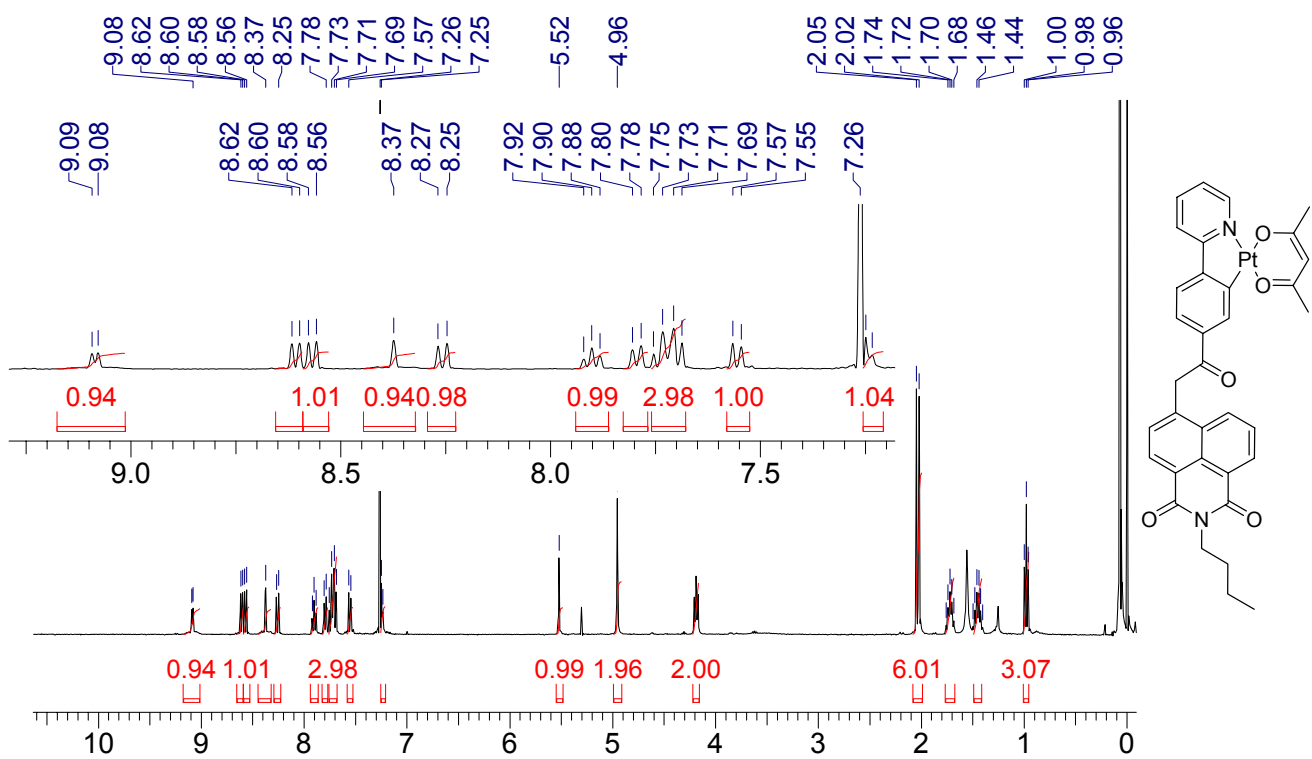


Fig. S10 ^1H NMR of Pt-2 (400 MHz, CDCl_3).

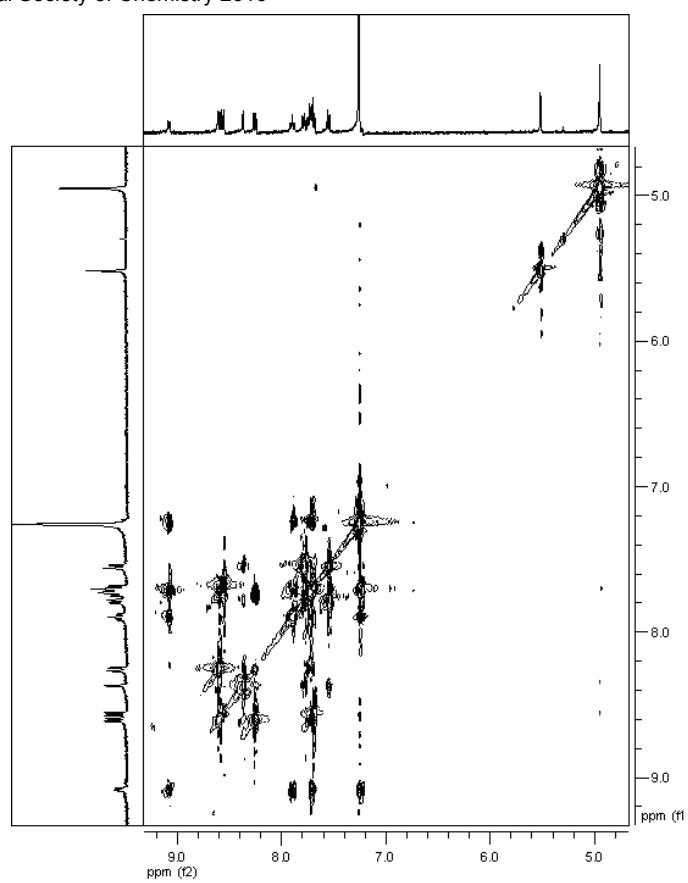


Fig. S11 TOCSY of Pt-2 (400 MHz, CDCl_3).

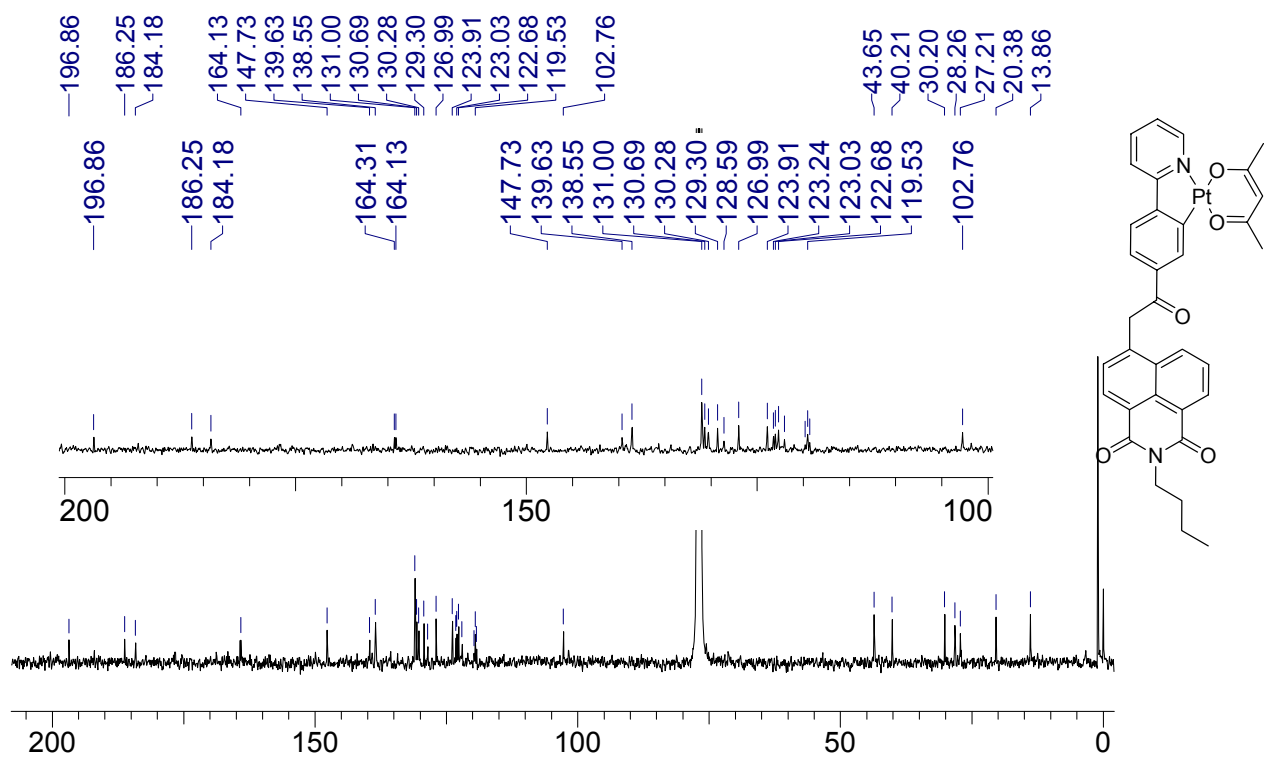


Fig. S12 ^{13}C NMR of Pt-2 (100 MHz, CDCl_3).

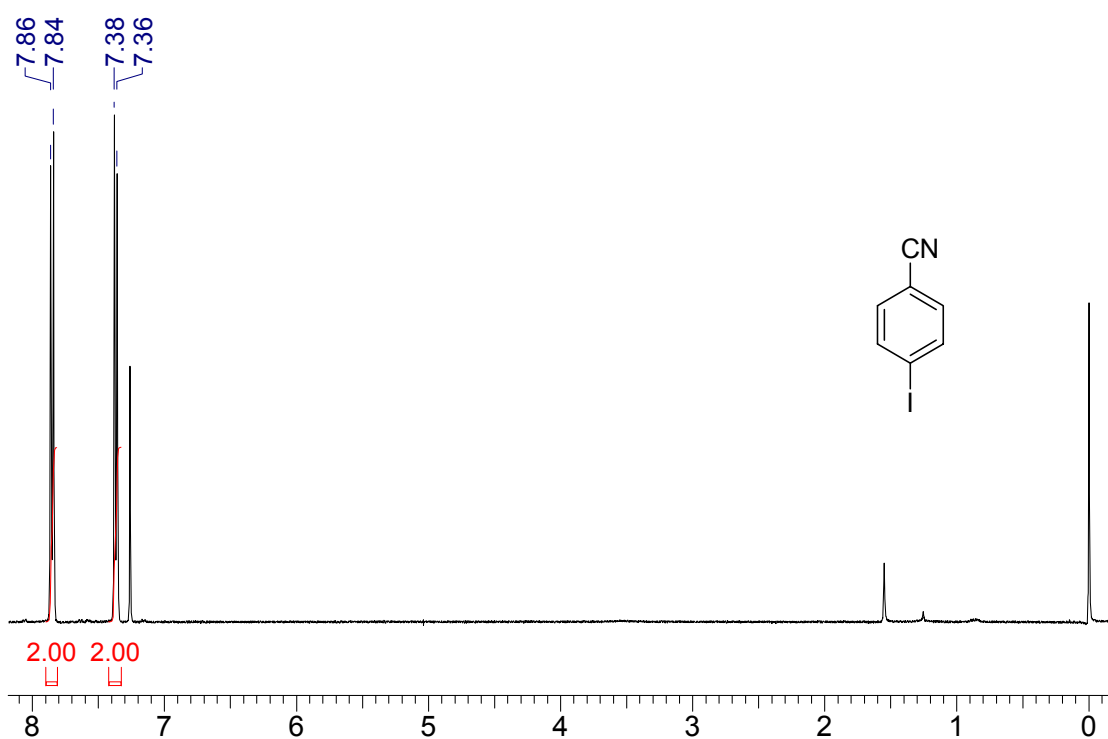


Fig. S13 ^1H NMR of **4** (400 MHz, CDCl_3).

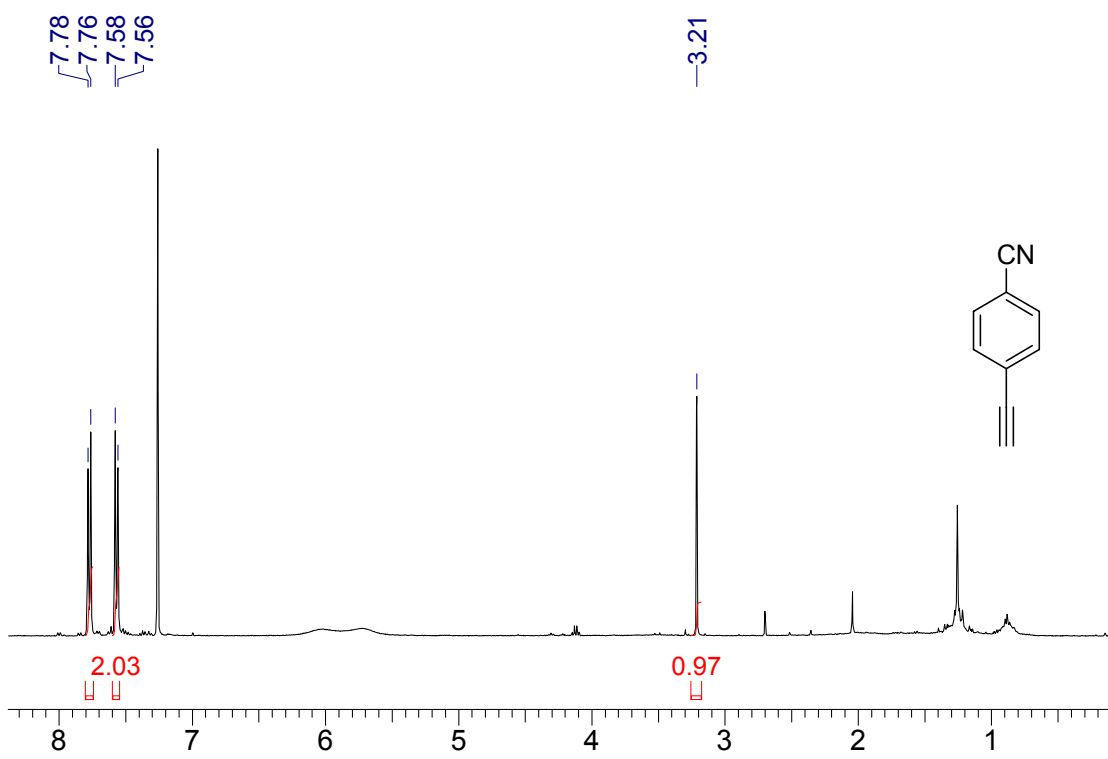


Fig. S14 ^1H NMR of **5** (400 MHz, CDCl_3).

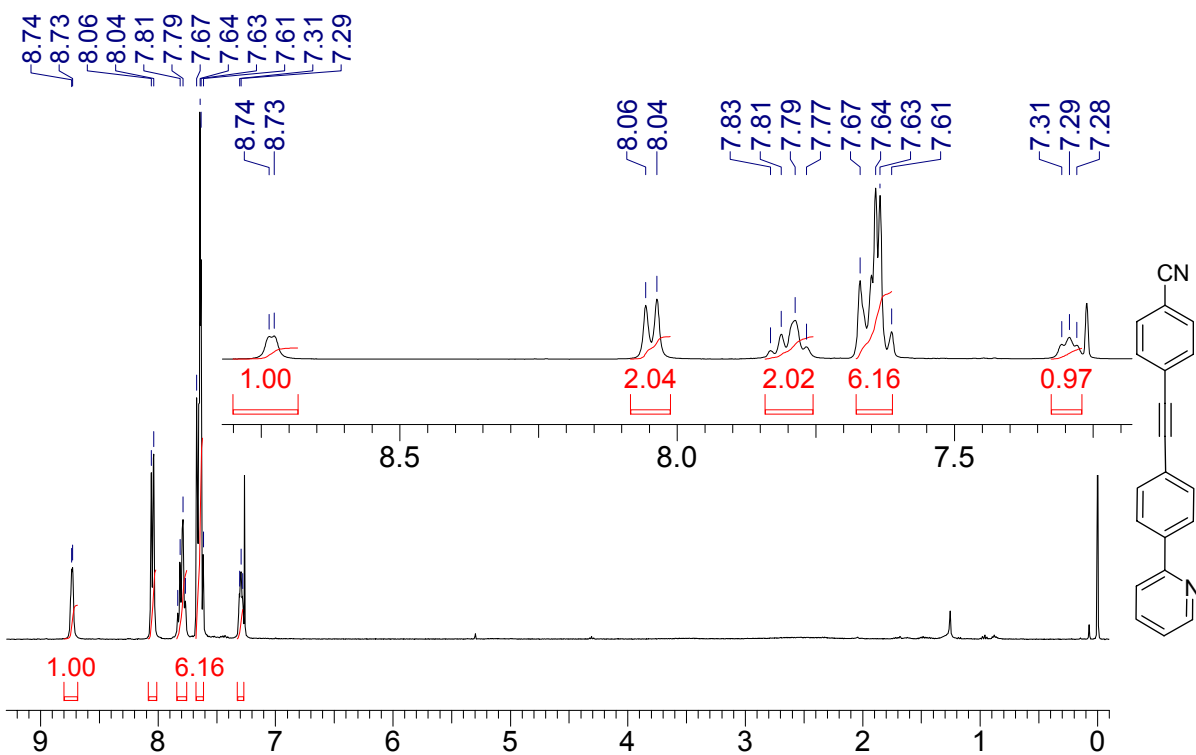


Fig. S15 ¹H NMR of L2 (400 MHz, CDCl₃).

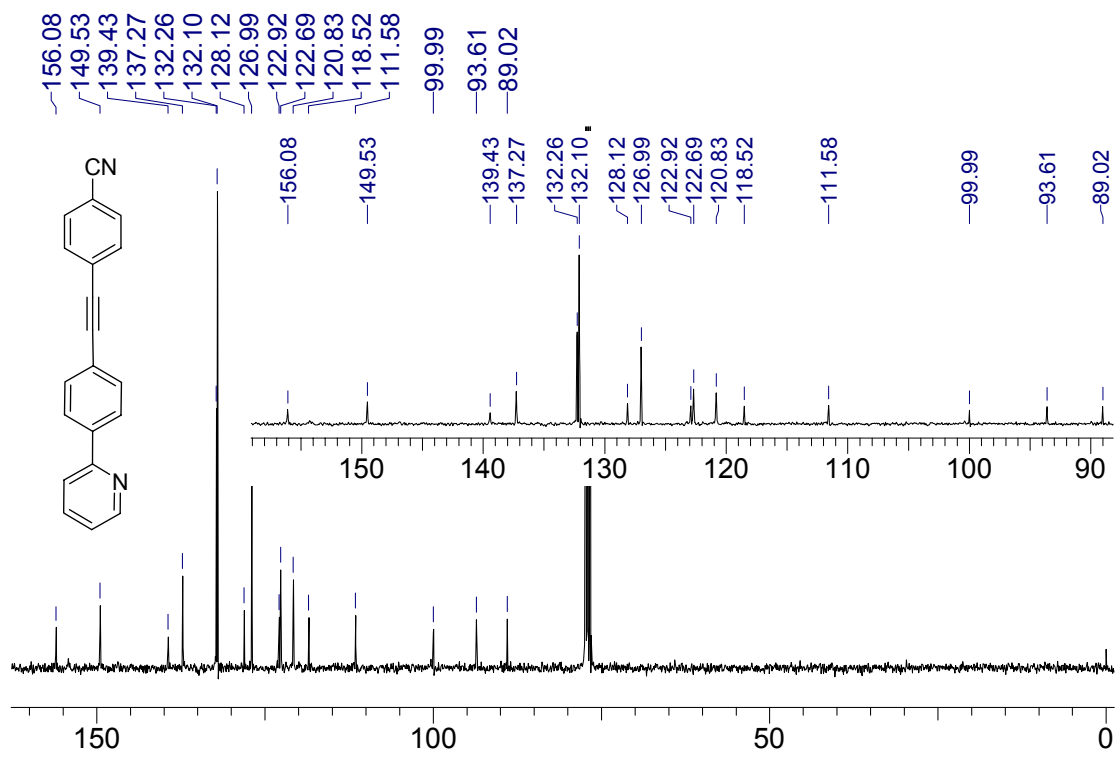


Fig. S16 ¹³C NMR of L2 (400MHz, CDCl₃).

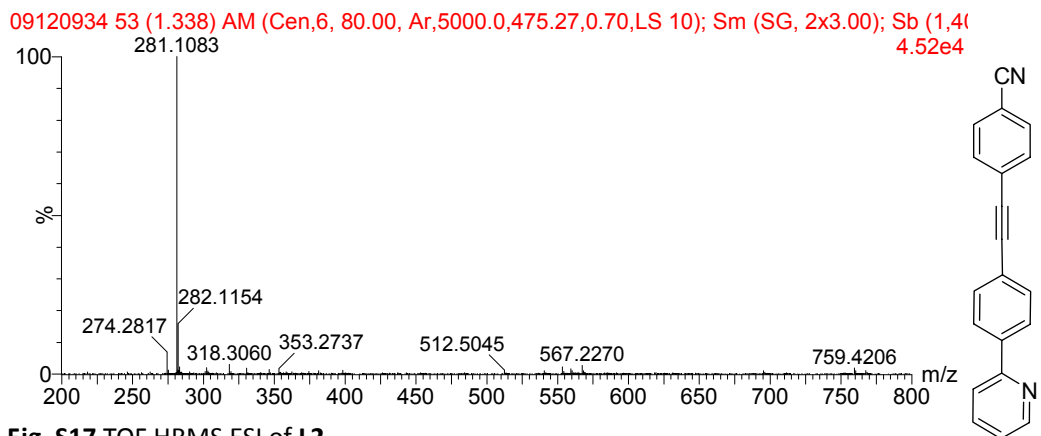


Fig. S17 TOF HRMS ESI of L2.

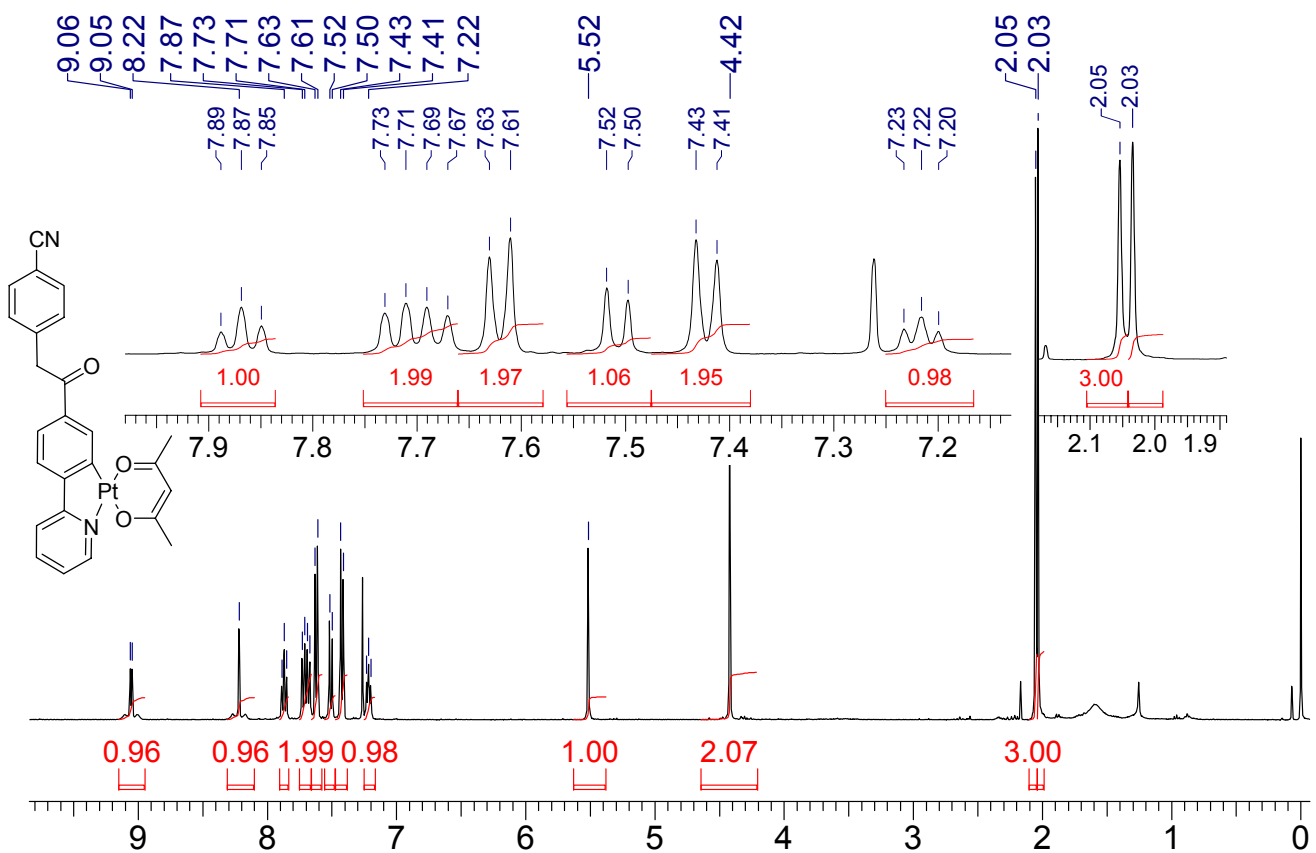


Fig. S18 ^1H NMR of Pt-3 (400 MHz, CDCl_3).

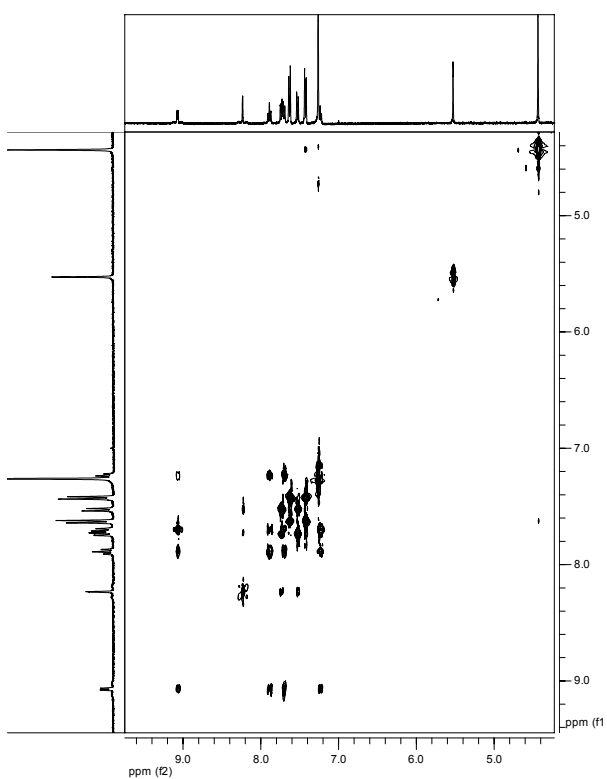


Fig. S19 TOCSY of Pt-3 (400MHz, CDCl₃).

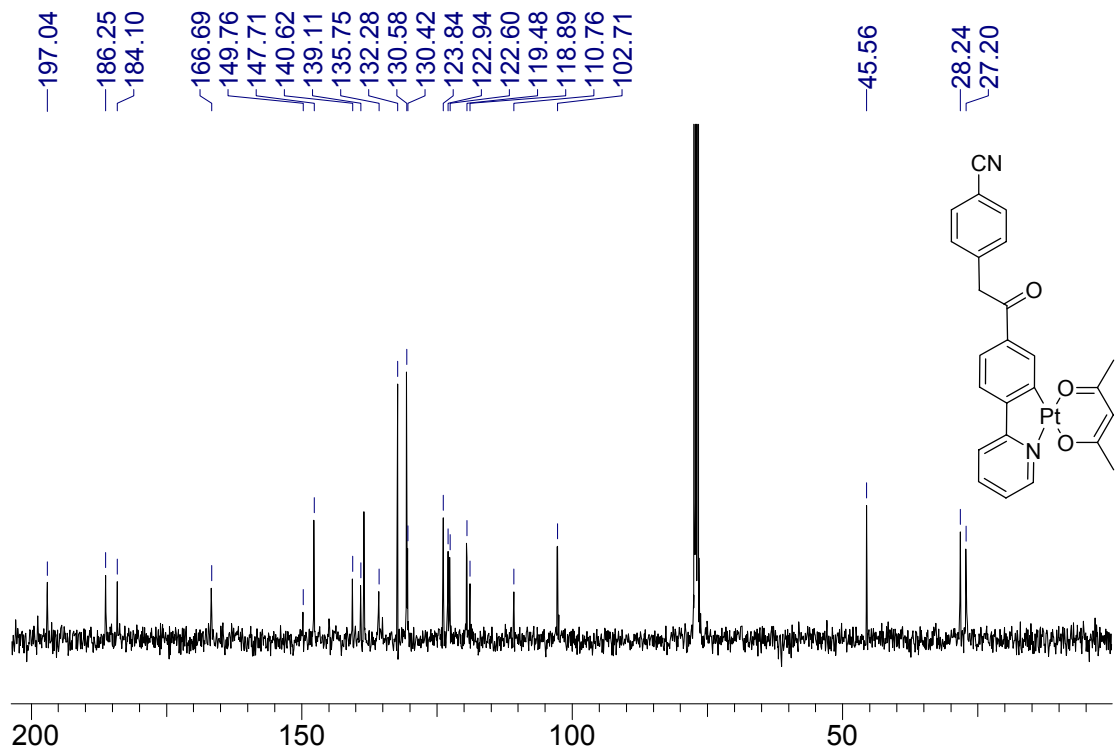


Fig. S20 ¹³C NMR of Pt-3 (100 MHz, CDCl₃).

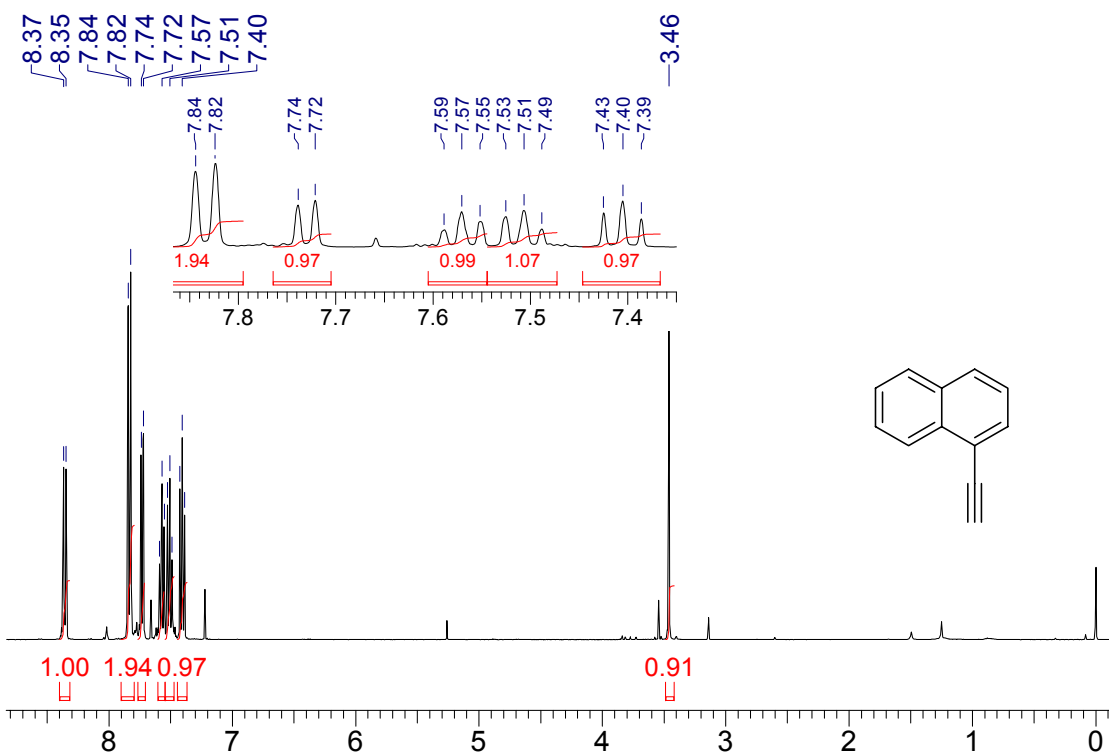


Fig. S21 ^1H NMR of 1-ethynylnaphthalene (**6**) (400 MHz, CDCl_3).

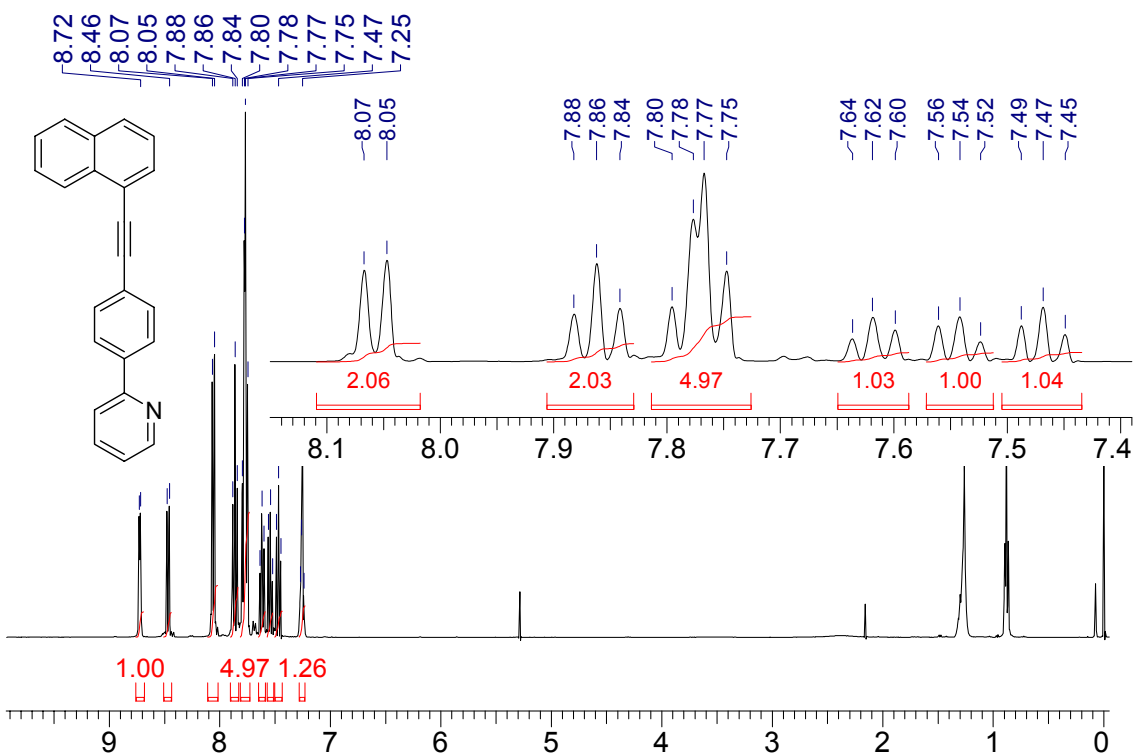


Fig. S22 ^1H NMR of **L3** (400 MHz, CDCl_3).

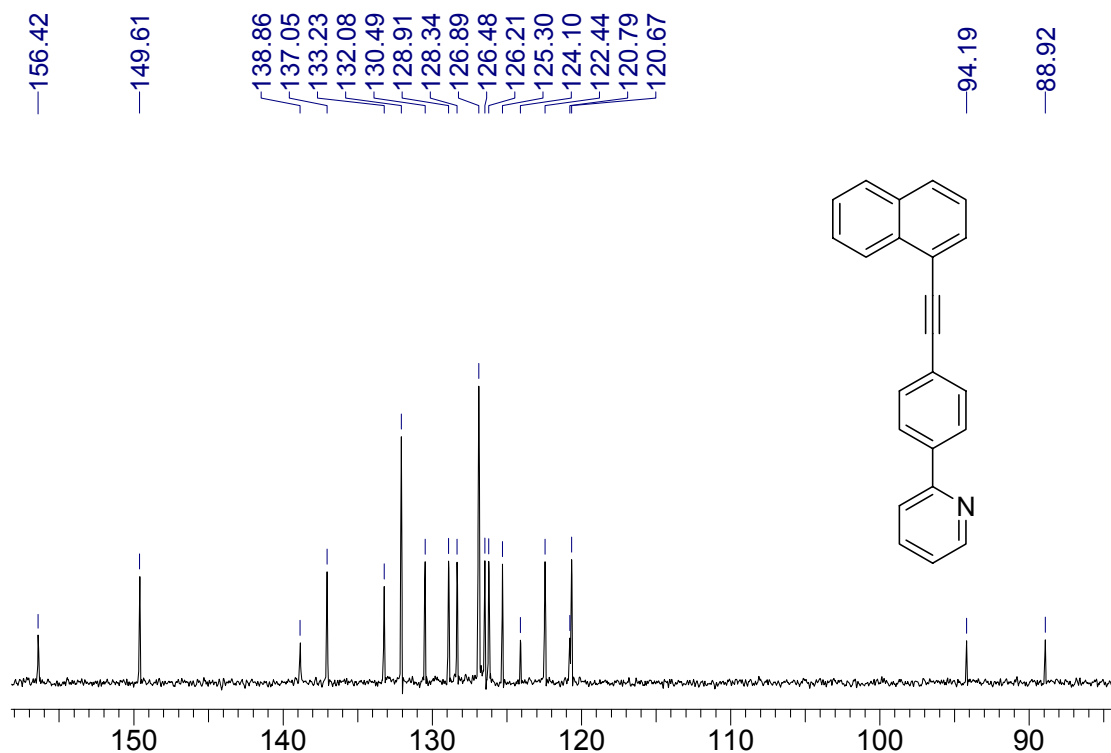


Fig. S23 ^{13}C NMR of L3 (100 MHz, CDCl_3).

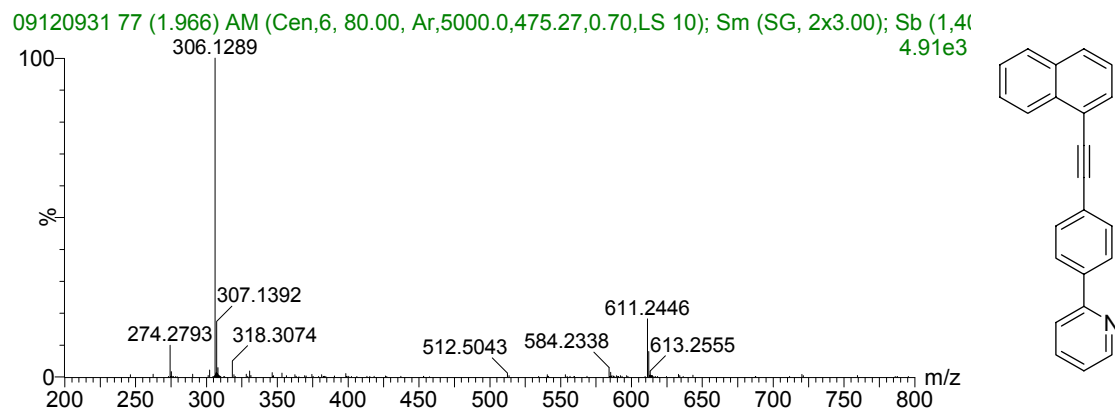


Fig. S24 TOF HRMS ESI of L3.

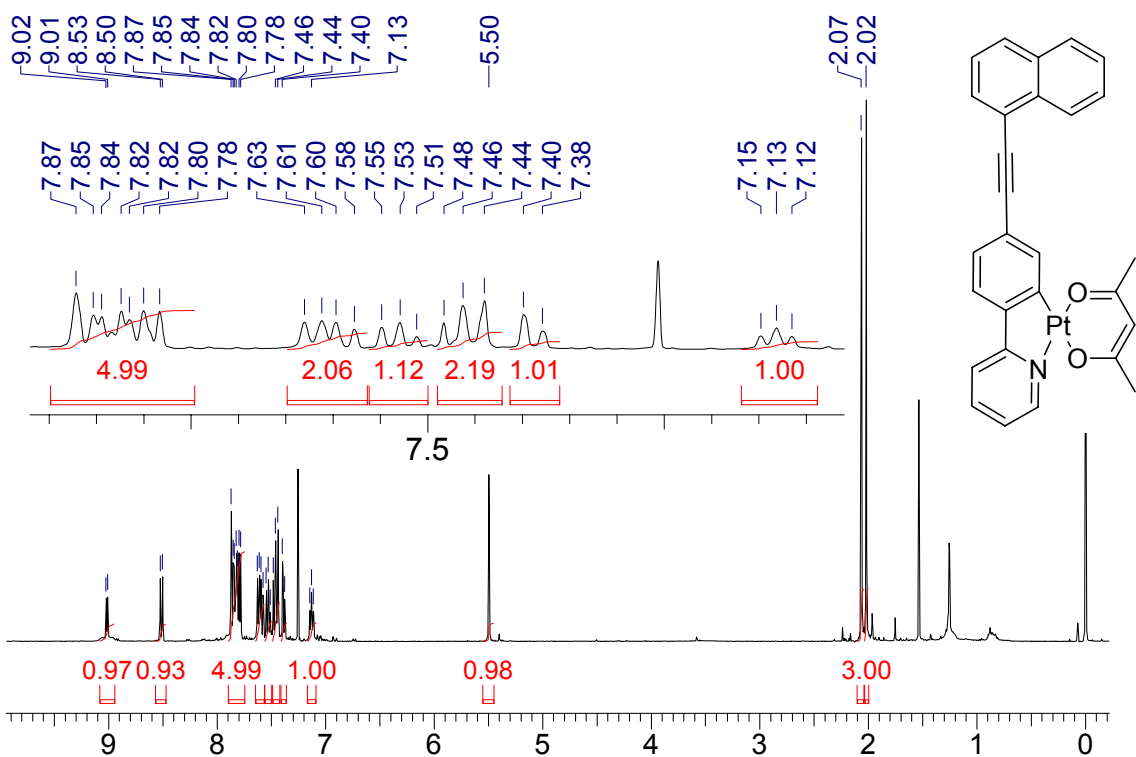


Fig. S25 ^1H NMR of Pt-4 (400MHz, CDCl_3).

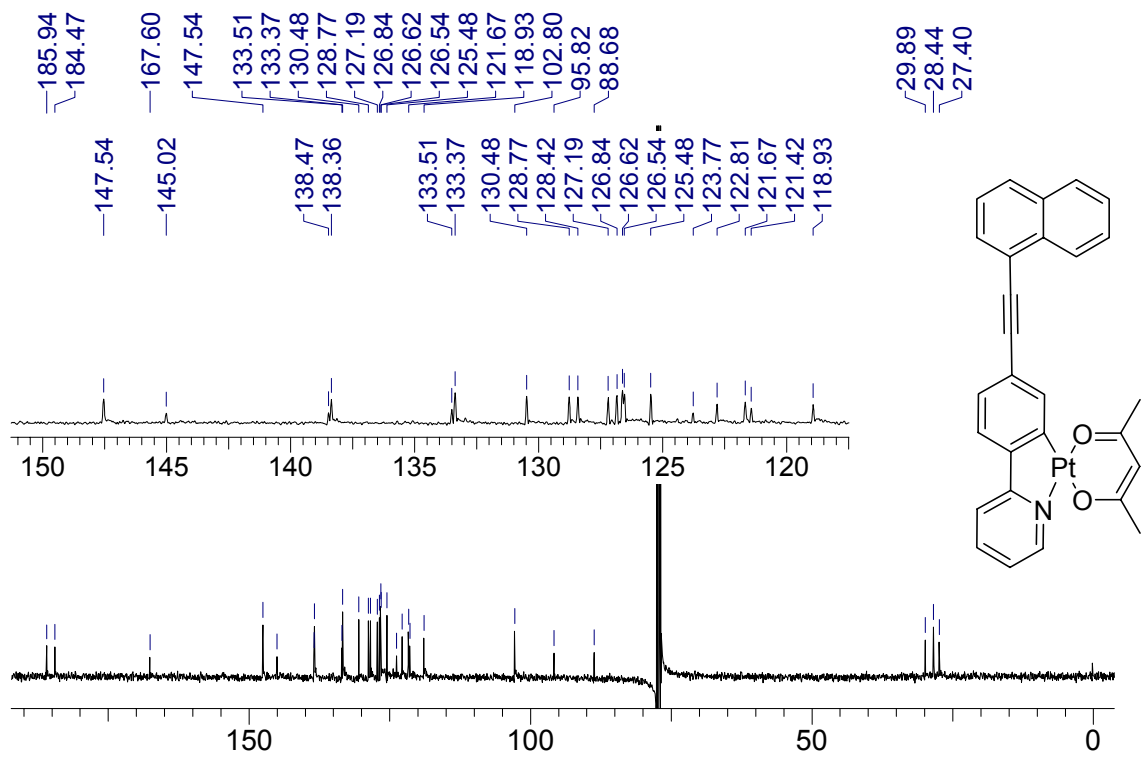


Fig. S26 ^{13}C NMR of Pt-4 (100 MHz, CDCl_3).

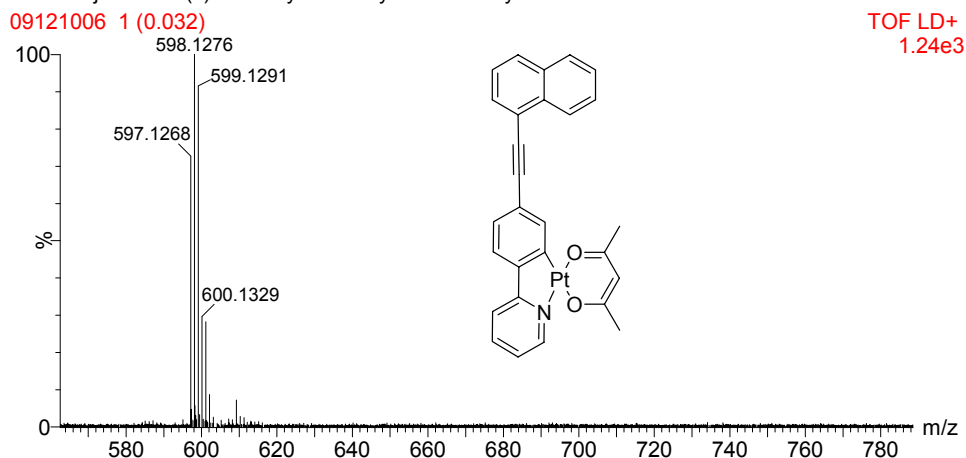


Fig. S27 MALDI-MS of Pt-4.

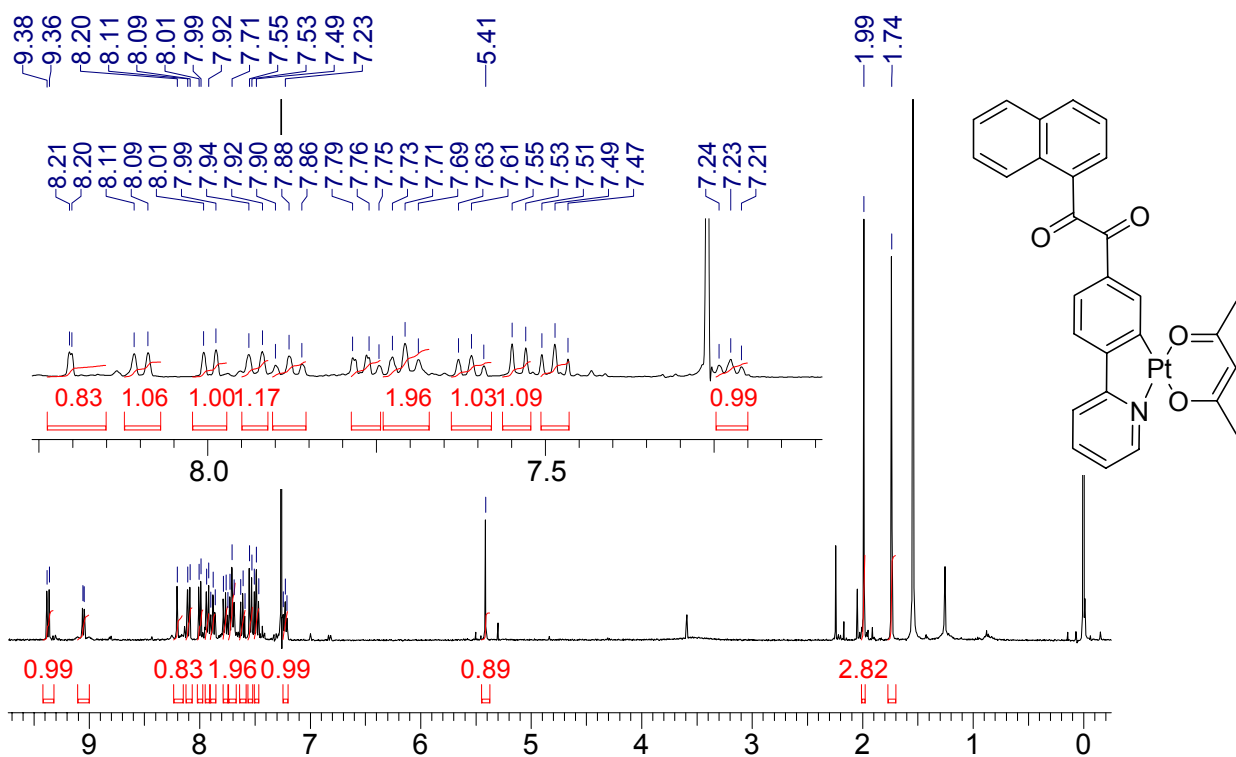


Fig. S28 ^1H NMR of Pt-5 (400MHz, CDCl_3).

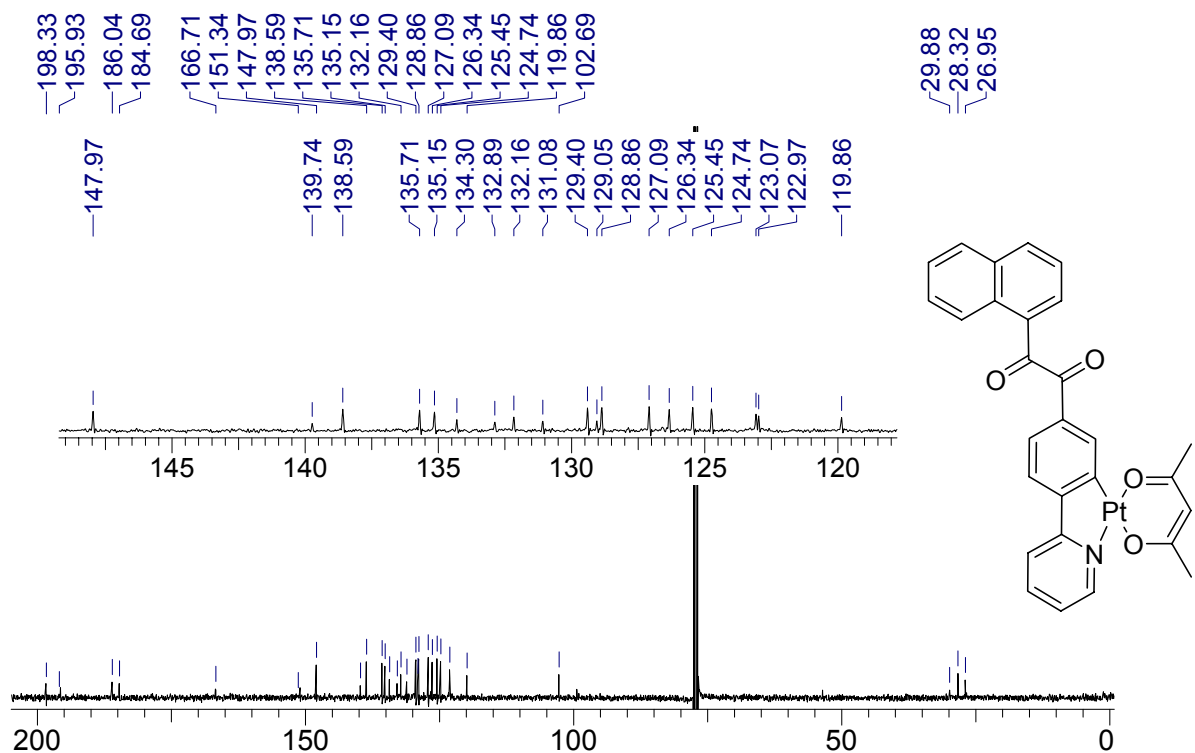


Fig. S29 ^{13}C NMR of Pt-5 (100 MHz, CDCl_3).

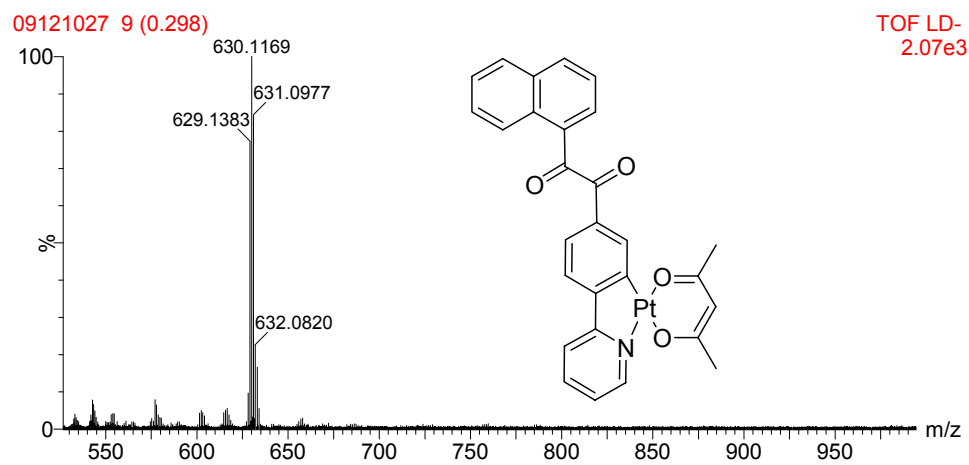


Fig. S30 MALDI-MS of Pt-5.

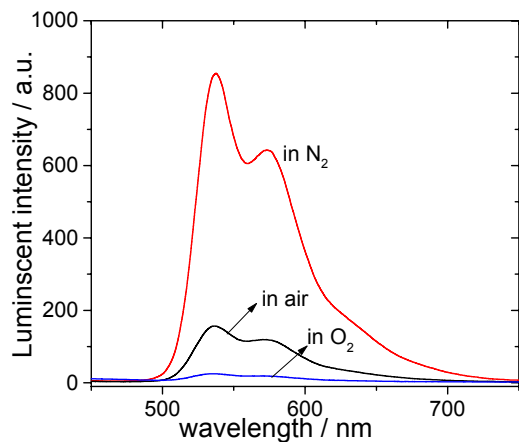


Fig. S31 Emission of complexes in solution under different atmosphere of Ar, air and oxygen. **Pt-3**, $\lambda_{\text{ex}} = 400 \text{ nm}$. The solution is purged with Ar or O₂ for about 20 min before measurement. $1.0 \times 10^{-5} \text{ mol dm}^{-3}$ in DCM. 20 °C.

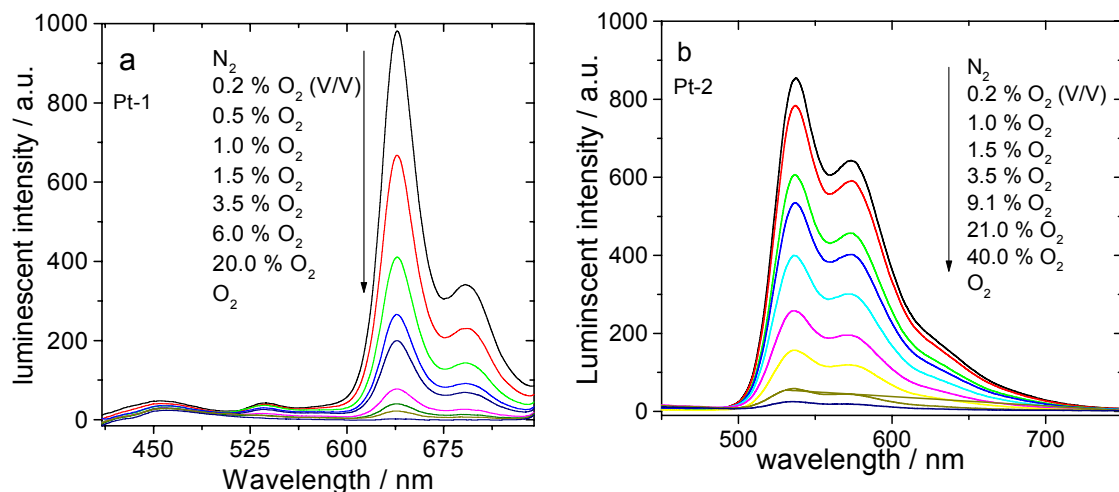


Fig. S32 Emission of complexes **Pt-1** and **Pt-3** in solution under different concentration of oxygen ($1.0 \times 10^{-5} \text{ mol dm}^{-3}$ in DCM),(a) **Pt-1**, $\lambda_{\text{ex}} = 390 \text{ nm}$.(b) **Pt-2** $\lambda_{\text{ex}} = 400 \text{ nm}$. The solution is purged with Ar or O₂ for about 20 min before measurement. 20 °C.

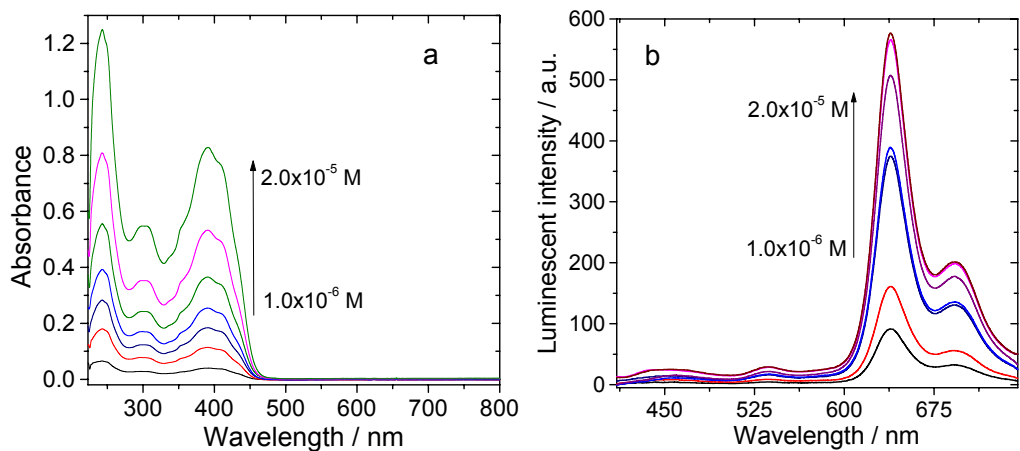


Fig. S33 (a) UV-Vis absorption spectra of **Pt-1** at different concentration in CH_2Cl_2 (from 1.0×10^{-6} M to 2.0×10^{-5} M). (b) Emission of complex **Pt-1** at different concentration in CH_2Cl_2 (from 1.0×10^{-6} M to 2.0×10^{-5} M) under Ar atmosphere. $\lambda_{\text{ex}} = 390$ nm.

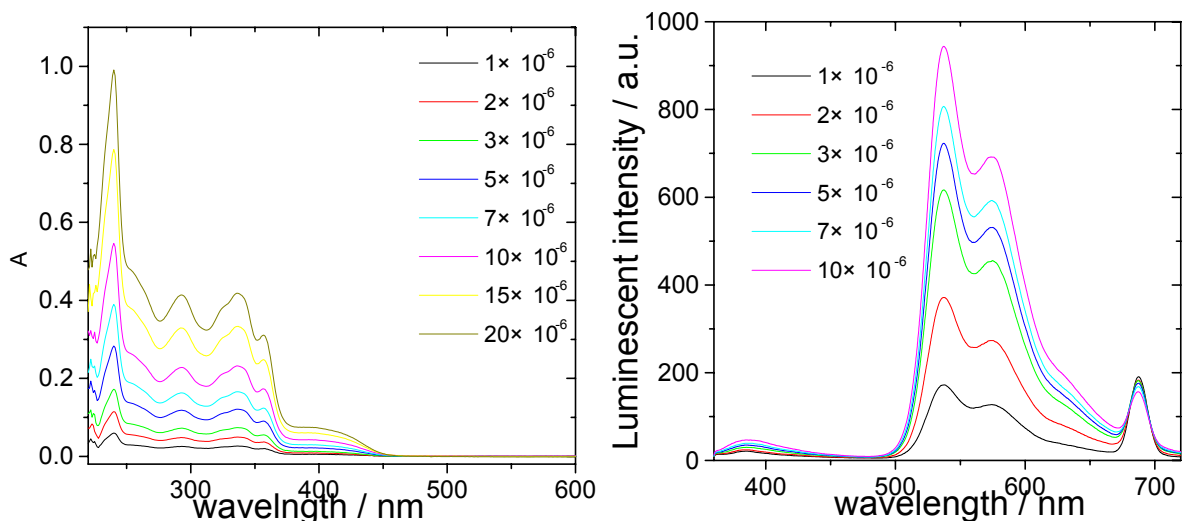


Fig. S34 (a) UV-Vis absorption spectra of **Pt-2** at different concentration in CH_2Cl_2 (from 1.0×10^{-6} M to 2.0×10^{-5} M). (b) Emission of complex **Pt-2** at different concentration in CH_2Cl_2 (from 1.0×10^{-6} M to 1.0×10^{-5} M) under Ar atmosphere. $\lambda_{\text{ex}} = 350$ nm.

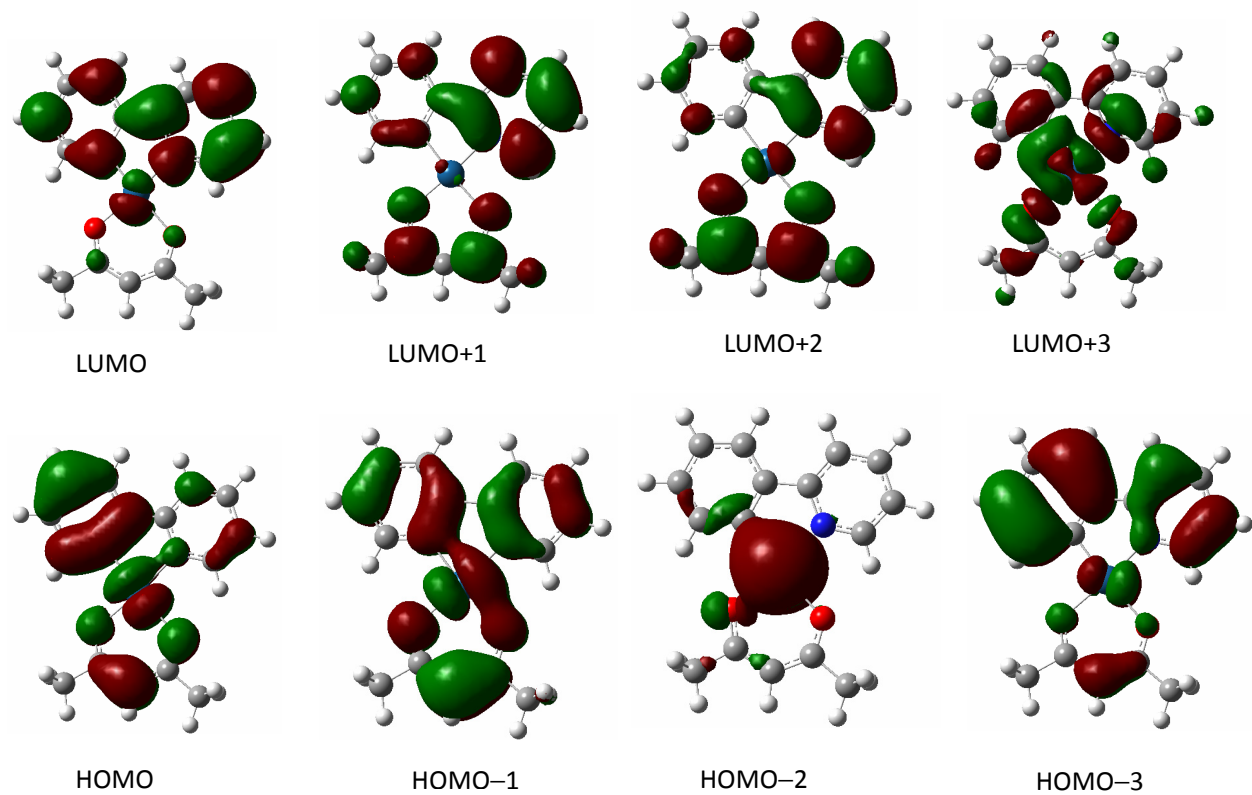


Fig. S35 Frontier molecular orbital for (ppy)Pt(acac). Calculated by DFT at the B3LYP/6-31G((d)/ LanL2DZ level

using Gaussian 09.

Table S1. Electronic Excitation Energies (eV) and corresponding Oscillator Strengths (*f*), main configurations and CI coefficients of the Low-lying Electronically Excited States of complex (*ppy*)Pt(acac), Calculated by TDDFT//B3LYP/6-31G(d)/LanL2DZ, based on the DFT//B3LYP/6-31G(d)/ LanL2DZ Optimized Ground State Geometries.

Electronic transition		TDDFT//B3LYP/6-31G(d)			
	Energy ^a	<i>f</i> ^b	Composition ^c	CI ^d	character
Singlet	$S_0 \rightarrow S_1$	3.12 eV 397 nm	HOMO–1→LUMO	0.21651	LLCT
			HOMO→LUMO	0.64243	ILCT, LLCT
	$S_0 \rightarrow S_2$	3.49 eV 355 nm	HOMO–2→LUMO	0.62316	MLCT
	$S_0 \rightarrow S_3$	3.53 eV 351 nm	HOMO–1→LUMO	0.62124	LLCT
			HOMO→LUMO	0.21200	ILCT, LLCT
			HOMO→LUMO+1	0.17675	MLCT, ILCT
			HOMO–3→ LUMO	0.19501	ILCT
			HOMO–3→LUMO+1	0.10457	ILCT, LLCT
Triplet	$S_0 \rightarrow T_1$	2.65 eV 467 nm	HOMO–1→ LUMO	0.37509	LLCT
			HOMO→ LUMO	0.57424	ILCT, LLCT
			HOMO→ LUMO+1	0.10573	MLCT, ILCT
			HOMO→ LUMO+4	0.10409	LLCT

^a Only the selected low-lying excited states are presented. ^b oscillator strength. ^c Only the main configurations are presented. ^d The CI coefficients are in absolute values. ^e No spin-orbital coupling effect was considered, thus the f values are zero.

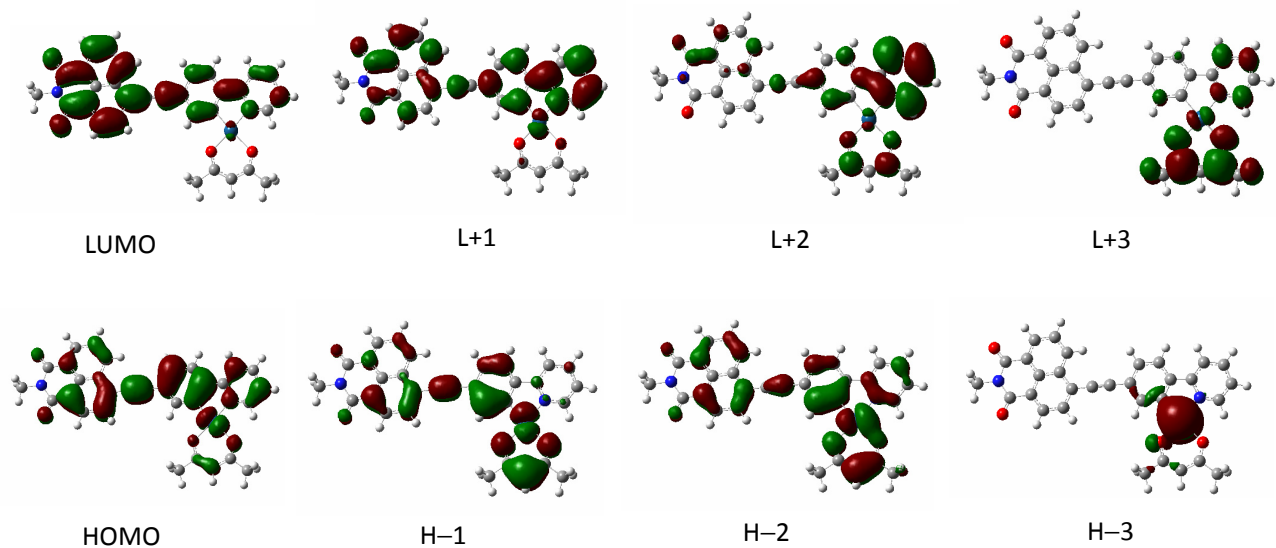


Fig. S36 Frontier molecular orbitals of **Pt-1**. H stands for HOMO and L stands for LUMO. Calculated by DFT at the B3LYP/6-31G((d)/ LanL2DZ level using Gaussian 09.

Table S2. Electronic Excitation Energies (eV) and corresponding Oscillator Strengths (f), main configurations and CI coefficients of the Low-lying Electronically Excited States of complex **Pt-1**, Calculated by TDDFT//B3LYP/6-31G(d)/LanL2DZ, based on the DFT//B3LYP/6-31G(d)/LanL2DZ Optimized Ground State Geometries.

Electronic transition		TDDFT//B3LYP/6-31G(d)					
		Energy ^a	f ^b	Composition ^c	CI ^d	character	
Singlet	S0→S1	2.74 eV	452 nm	0.4456	H-2→L	0.1131	MLCT,LLCT, ILCT
					H-1→L	0.1651	MLCT,LLCT, ILCT
					H→L	0.6317	MLCT, ILCT
	S0→S2	2.89 eV	429 nm	0.4941	H-1→L	0.6560	MLCT,LLCT, ILCT
					H→L	0.1358	MLCT, ILCT
	S0→S3	3.14 eV	394 nm	0.1411	H-2→L	0.5607	MLCT,LLCT, ILCT
					H-2→L+1	0.2081	MLCT,LLCT
					H→L	0.1431	MLCT, ILCT
					H→L+1	0.2632	MLCT,LLCT
Triplet	S0→T1	1.86 eV	666 nm	0.0000e	H-4→L	0.1478	ILCT
					H-4→L+1	0.1493	ILCT
					H-2→L	0.2110	MLCT,LLCT, ILCT
					H-1→L	0.3419	MLCT,LLCT, ILCT
					H→L	0.6331	MLCT, ILCT

^a Only the selected low-lying excited states are presented. ^b oscillator strength. ^c H stands for HOMO and L stands for LUMO. Only the main configurations are presented. ^d The CI coefficients are in absolute values. ^e No spin-orbital coupling effect was considered, thus the f values are zero.

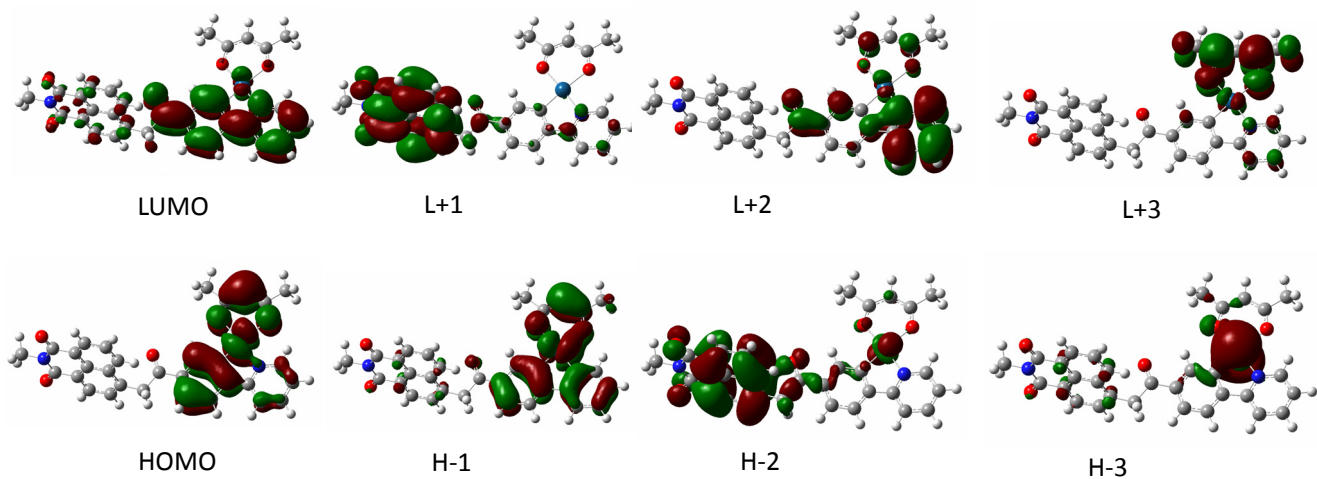


Fig. S37 Frontier molecular orbitals of **Pt-2**. H stands for HOMO and L stands for LUMO. Calculated by DFT at the B3LYP/6-31G((d))/ LanL2DZ level using Gaussian 09.

Table S3. Electronic Excitation Energies (eV) and corresponding Oscillator Strengths (f), main configurations and CI coefficients of the Low-lying Electronically Excited States of complex **Pt-2**, Calculated by TDDFT//B3LYP/6-31G(d)/LanL2DZ, based on the DFT//B3LYP/6-31G(d)/LanL2DZ Optimized Ground State Geometries.

Electronic transition		TDDFT//B3LYP/6-31G(d)				
		Energy (eV) ^a	f ^b	Composition ^c	CI ^d	character
Singlet	S0→S1	2.93 eV 423 nm	0.0498	H-1→L	0.2357	LLCT MLCT
				H→L	0.6092	LLCT
				H→L+1	0.1304	ILCT, LLCT,MLCT
	S0→S2	3.17 eV 391 nm	0.0446	H-1→L	0.5954	LLCT MLCT
				H→L	0.2488	LLCT
				H-1→L+1	0.1282	ILCT,LLCT
	S0→S7	3.64 eV 341 nm	0.2859	H-2→L+1	0.5641	MLCT
				H-2→L	0.2040	ILCT
				H-1→L+1	0.1913	ILCT,LLCT
	S0→S22	4.22 eV 294 nm	0.2931	H-1→L+3	0.3191	LLCT
				H-7→L	0.3390	LLCT, MLCT
				H-4→L	0.2645	LLCT
				H-4→L+1	0.2144	ILCT, LLCT
				H-1→L+3	0.2243	LLCT,MLCT
Triplet	S0→T ₁	2.29 eV 541 nm	0.0000 ^e	H-2→L+1	0.7118	MLCT
				H-2→L	0.2058	LLCT,MLCT
				H-1→L+1	0.1585	ILCT,LLCT
				H-3→L+1	0.1530	MLCT

^a Only the selected low-lying excited states are presented. ^b oscillator strength. ^c H stands for HOMO and L stands for LUMO. Only the main configurations are presented. ^d The CI coefficients are in absolute values. ^e No spin-orbital coupling effect was considered, thus the f values are zero.

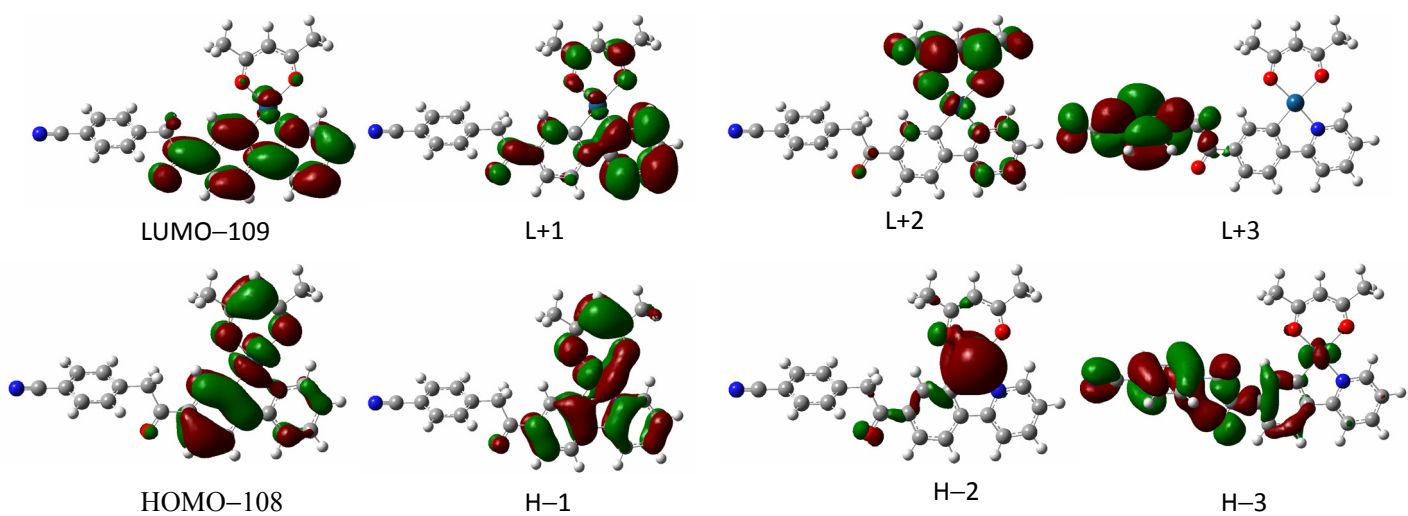


Fig. S38 Frontier molecular orbital for **Pt-3**. Calculated by DFT at the B3LYP/6-31G((d)/ LanL2DZ level using Gaussian 09.

Table S4. Electronic Excitation Energies (eV) and corresponding Oscillator Strengths (*f*), main configurations and CI coefficients of the Low-lying Electronically Excited States of complex **Pt-3**, Calculated by TDDFT//B3LYP/6-31G(d)/LanL2DZ, based on the DFT//B3LYP/6-31G(d)/ LanL2DZ Optimized Ground State Geometries.

Electronic transition		TDDFT//B3LYP/6-31G(d)				
		Energy ^a	<i>f</i> ^b	Composition ^c	CI ^d	character
Singlet	$S_0 \rightarrow S_1$	2.96 eV 418 nm	0.0560	HOMO-1→LUMO	0.20956	MLCT, LLCT
				HOMO→LUMO	0.63211	MLCT, LLCT, ILCT
				HOMO-2→LUMO	0.17326	MLCT
	$S_0 \rightarrow S_3$	3.26 eV 380 nm	0.0486	HOMO-1→LUMO	0.62690	MLCT, LLCT
				HOMO→LUMO	0.21588	MLCT, LLCT, ILCT
				HOMO-6→LUMO	0.25770	MLCT, LLCT
	$S_0 \rightarrow S_{13}$	4.23 eV 293 nm	0.2118	HOMO-5→LUMO	0.24341	ILCT
				HOMO-4→LUMO	0.27281	ILCT
				HOMO-1→LUMO+1	0.31459	LLCT
				HOMO-1→LUMO+2	0.33672	MLCT, LLCT
				HOMO-4→LUMO	0.17965	ILCT
				HOMO-1→LUMO+1	0.37069	LLCT
Triplet	$S_0 \rightarrow T_1$	2.41 eV 515 nm	0.0000	HOMO→LUMO	0.60752	MLCT, LLCT, ILCT
				HOMO-6→LUMO	0.22603	ILCT
				HOMO-4→LUMO	0.15205	ILCT
	$S_0 \rightarrow T_2$	2.81 eV 442 nm	0.0000	HOMO-4→LUMO+1	0.44021	MLCT, LLCT, ILCT
				HOMO-1→LUMO	0.22065	ILCT
				HOMO→LUMO	0.49713	MLCT, LLCT, ILCT

^a Only the selected low-lying excited states are presented. ^b oscillator strength. ^c Only the main configurations are presented. ^d The CI coefficients are in absolute values. ^e No spin-orbital coupling effect was considered, thus the f values are zero.

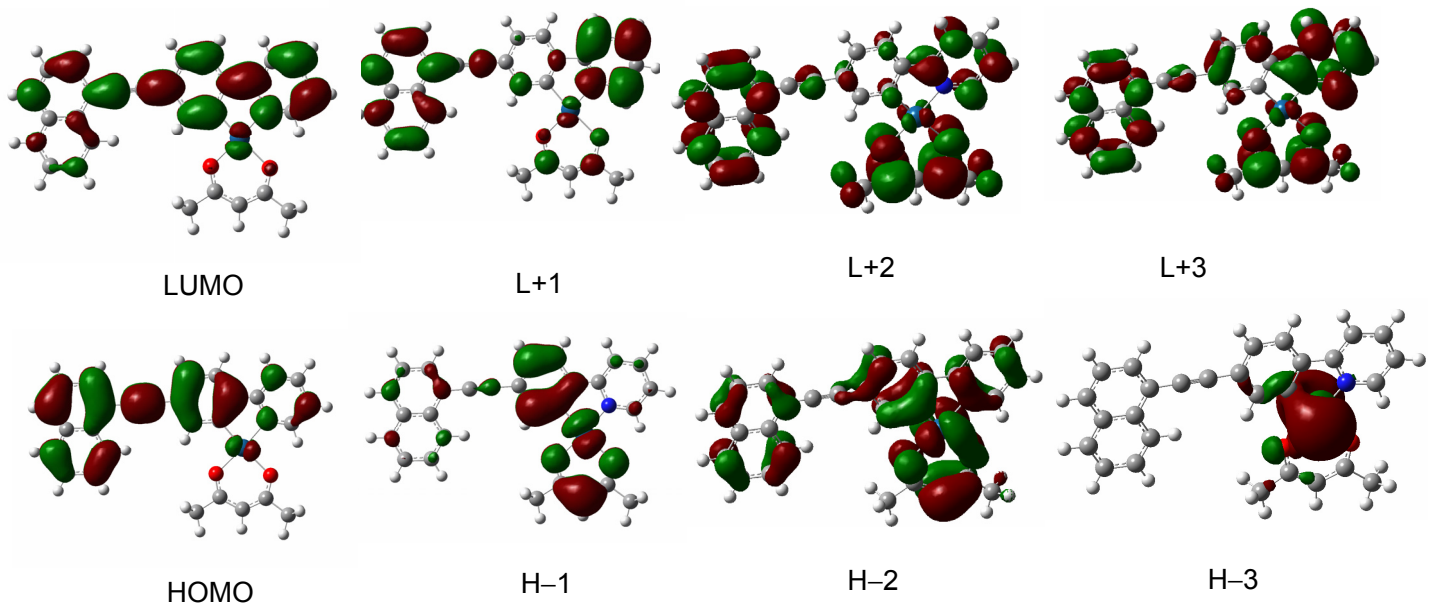


Fig. S39 Frontier molecular orbital for **Pt-4**. Calculated by DFT at the B3LYP/6-31G((d)/ LanL2DZ level using Gaussian 09.

Table S5. Electronic Excitation Energies (eV) and corresponding Oscillator Strengths (*f*), main configurations and CI coefficients of the Low-lying Electronically Excited States of complex **Pt-4**, Calculated by TDDFT//B3LYP/6-31G(d)/LanL2DZ, based on the DFT//B3LYP/6-31G(d)/LanL2DZ Optimized Ground State Geometries.

Electronic transition		TDDFT//B3LYP/6-31G(d)				
		Energy (eV) ^a	<i>f</i> ^b	Composition ^c	CI ^d	character
Singlet	$S_0 \rightarrow S_1$	2.94 eV/421 nm	0.4676	H→L	0.5804	ILCT
				H-1→L	0.2412	LLCT/MLCT
				H-2→L	0.1809	ILCT
	$S_0 \rightarrow S_2$	3.13 eV/396 nm	0.2758	H→L	0.2755	ILCT
				H-1→L	0.6128	LLCT/MLCT
	$S_0 \rightarrow S_5$	3.55 eV/349 nm	0.2108	H→L+1	0.6111	ILCT
Triplet	$S_0 \rightarrow T_1$	2.07 eV/599 nm	0.0000 ^e	H→L	0.6806	ILCT
				H→L+1	0.2657	ILCT

^a Only the selected low-lying excited states are presented. ^b oscillator strength. ^c H stands for HOMO and L stands for LUMO. Only the main configurations are presented. ^d The CI coefficients are in absolute values. ^e No spin-orbital coupling effect was considered, thus the f values are zero.

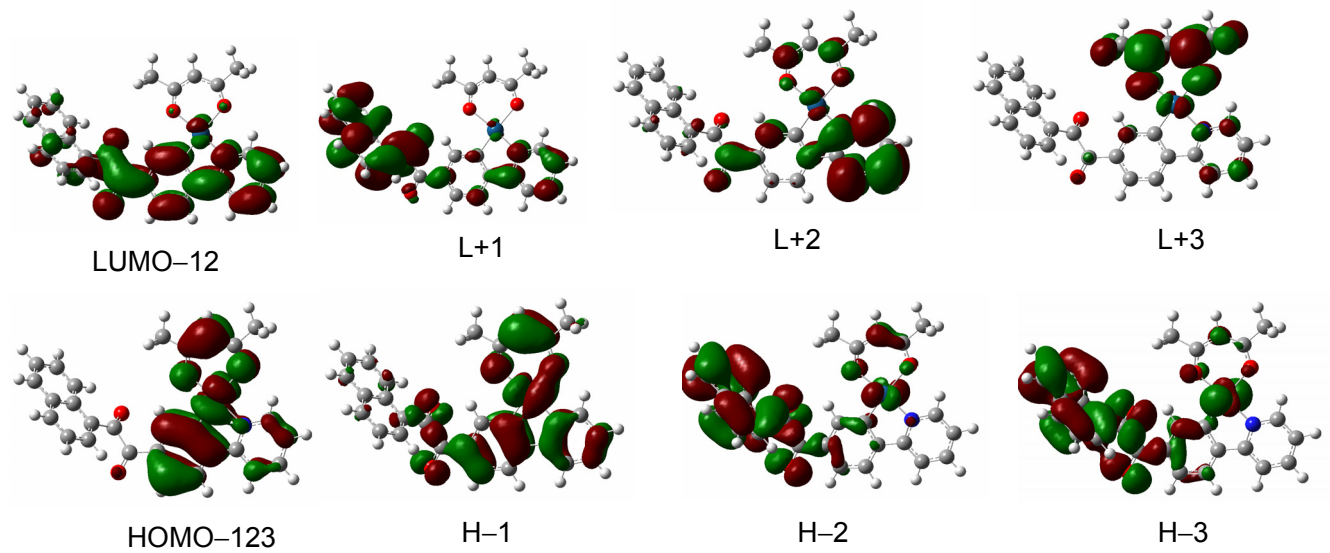


Fig. S40 Frontier molecular orbital for **Pt-5**. Calculated by DFT at the B3LYP/6-31G((d)/ LanL2DZ level using Gaussian 09.

Table S6. Electronic Excitation Energies (eV) and corresponding Oscillator Strengths (*f*), main configurations and CI coefficients of the Low-lying Electronically Excited States of complex **Pt-5**, Calculated by TDDFT//B3LYP/6-31G(d)/LanL2DZ, based on the DFT//B3LYP/6-31G(d)/LanL2DZ Optimized Ground State Geometries.

Electronic transition	TDDFT//B3LYP/6-31G(d)					
	Energy ^a	<i>f</i> ^b	Composition ^c	CI ^d	character	
Singlet	$S_0 \rightarrow S_1$	2.76 eV 448 nm	0.0020	HOMO–4→LUMO	0.1308	MLCT L'LCT
				HOMO–3→LUMO	0.4078	ILCT MLCT
				HOMO–2→LUMO	0.3511	ILCT
				HOMO–1→LUMO	0.2175	L'LCT MLCT
				HOMO→LUMO	0.1053	L'LCT MLCT
	$S_0 \rightarrow S_3$	3.14 eV 394 nm	0.0425	HOMO–2→LUMO	0.2307	ILCT
				HOMO–1→LUMO	0.5765	L'LCT MLCT
				HOMO→LUMO	0.2151	L'LCT MLCT
	$S_0 \rightarrow S_{10}$	3.75 eV 330 nm	0.1524	HOMO–5→LUMO	0.1879	$\pi \rightarrow \pi^*$ (ppy)/L'LCT
				HOMO–3→LUMO+1	0.5234	MLCT ILCT
				HOMO–1→LUMO+1	0.2556	L'LCT/MLCT/ILCT
	$S_0 \rightarrow S_{18}$	4.14 eV 299 nm	0.2012	HOMO–7→LUMO	0.3564	L'LCT MLCT
				HOMO–5→LUMO+1	0.2248	ILCT L'LCT
				HOMO–1→LUMO+2	0.2935	L'LCT MLCT
				HOMO–4→LUMO	0.1284	MLCT L'LCT
				HOMO–3→LUMO	0.2725	ILCT MLCT
Triplet	$S_0 \rightarrow T_1$	2.31 eV 537 nm	0.0000	HOMO–2→LUMO	0.2983	ILCT
				HOMO–2→LUMO+1	0.2981	ILCT
				HOMO–1→LUMO	0.3822	ILCT LLCT
				HOMO→LUMO	0.2525	L'LCT MLCT

^a Only the selected low-lying excited states are presented. ^b oscillator strength. ^c H stands for HOMO and L stands for LUMO. Only the main configurations are presented. ^d The CI coefficients are in absolute values. ^e L: diketo moiety; L': Hacac. ^f No spin-orbital coupling effect was considered, thus the f values are zero.

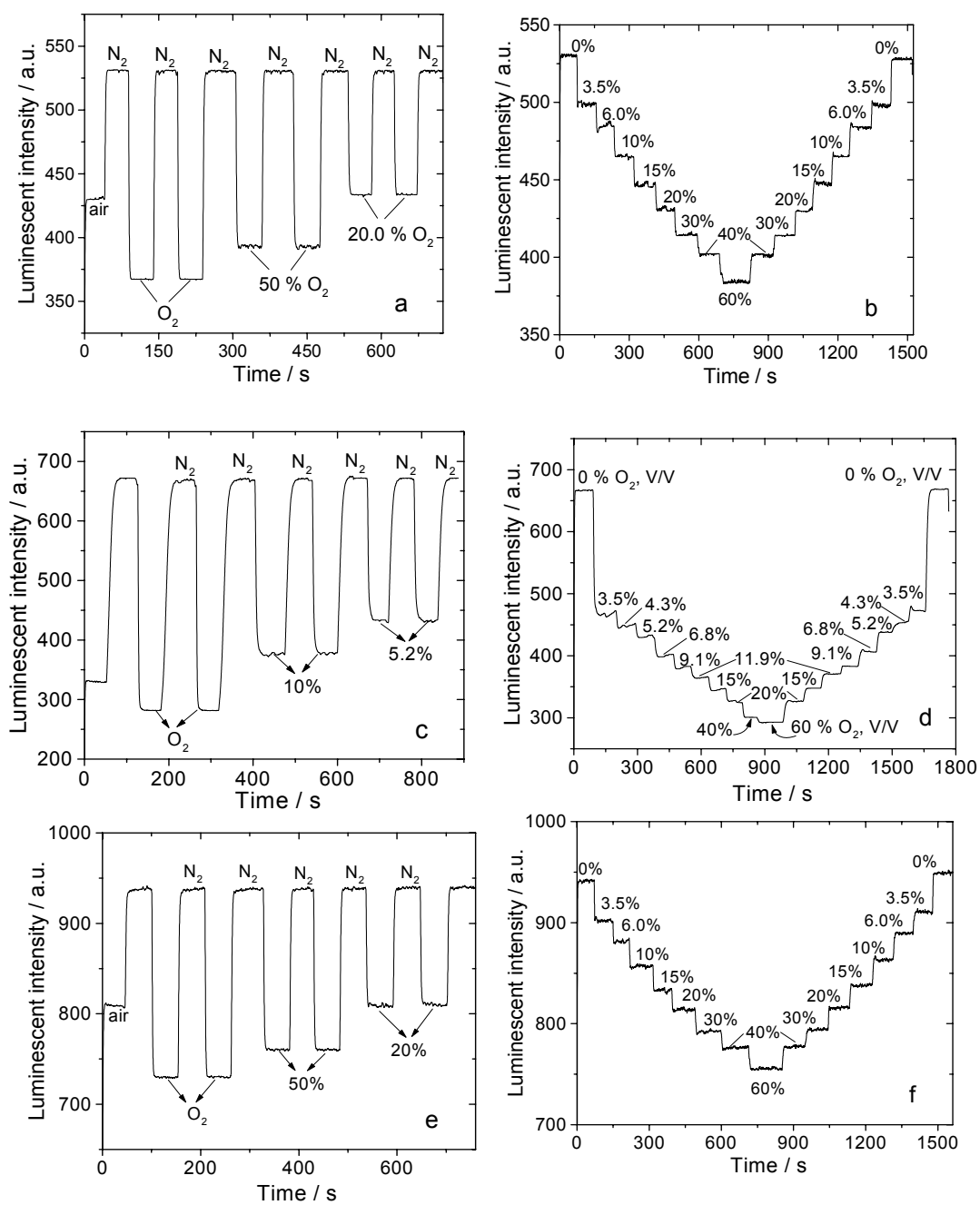


Fig. S41 Phosphorescent emission intensity response of the complexes to step variations of O_2 concentration levels. (a) and (b) **Pt-3**, excitation wavelength $\lambda_{\text{ex}} = 419 \text{ nm}$, emission wavelength $\lambda_{\text{em}} = 531 \text{ nm}$. (c) and (d) **Pt-4**, excitation wavelength $\lambda_{\text{ex}} = 403 \text{ nm}$, emission wavelength $\lambda_{\text{em}} = 569 \text{ nm}$. (e) and (f) **Pt-5** excitation wavelength $\lambda_{\text{ex}} = 423 \text{ nm}$, emission wavelength $\lambda_{\text{em}} = 539 \text{ nm}$.

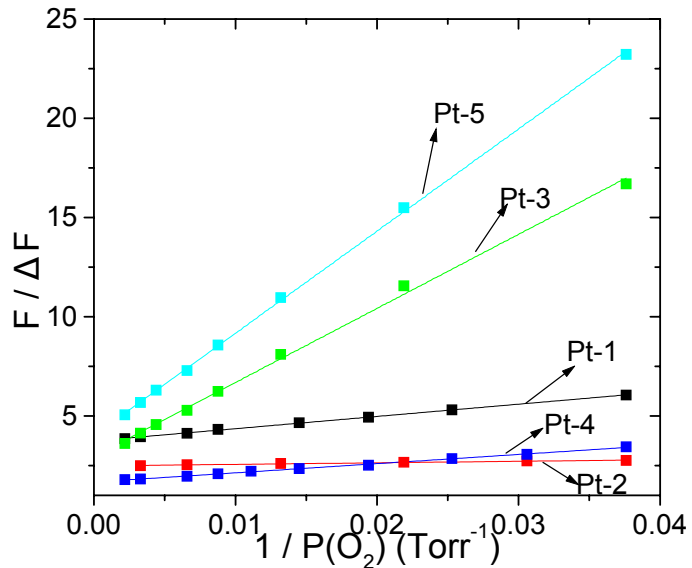


Fig. S42 Fitting of the oxygen sensing property of the IMPEK-C films of complex based on the modified Stern-Volmer equation.

Table S7. parameters of O₂ sensing film of complexes with IMPEK-C as supporting matrix (fitting result of the modified Stern-Volmer equation).

	f	K_{SV}	r^2	pO ₂ /Torr ^a
Pt-1	0.2673	0.0606	0.9993	16.5
Pt-2	0.4027	0.3212	0.9815	3.1
Pt-3	0.3383	0.0079	0.9975	126.6
Pt-4	0.5987	0.0361	0.9981	27.7
Pt-5	0.2486	0.0078	0.9996	128.2

^a The oxygen partial pressure at which the initial emission intensity of film is quenched by 50 %, and can be calculated as $1/K_{SV}$.

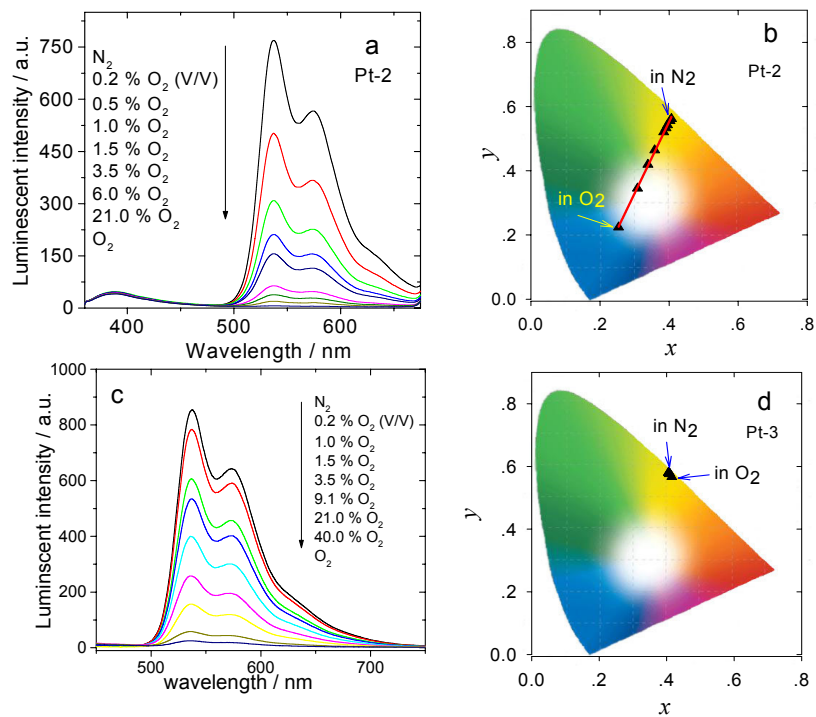
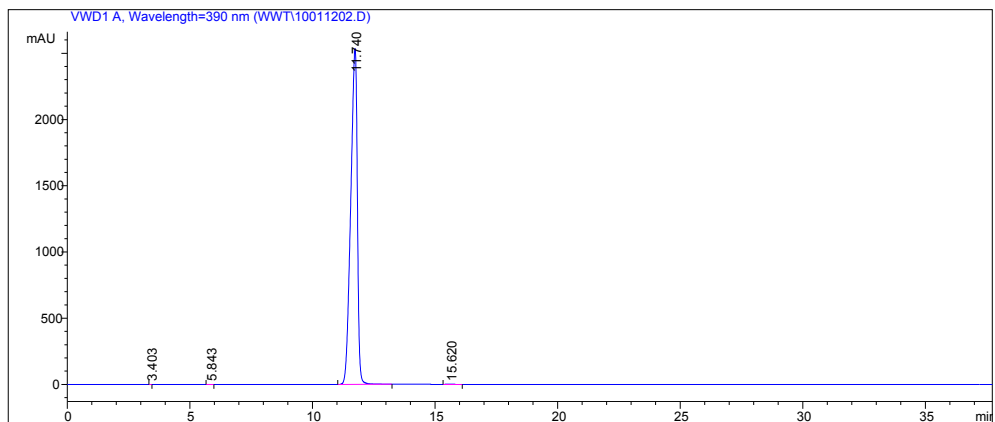


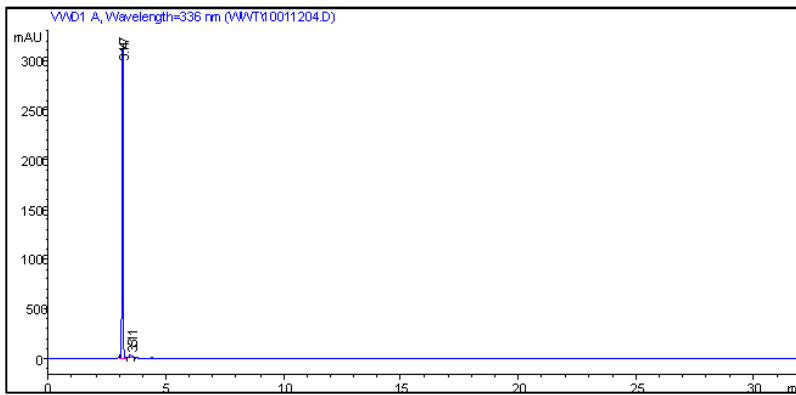
Fig. S43 CIE color coordinates of the ratiometric oxygen sensing. Emission of the complexes in solution under different oxygen concentration (1.0×10^{-5} mol dm⁻³ in dichloromethane). The solution is purged with Ar or mixed O₂/N₂ gas for about 20 min before measurement. (a) Pt-2, $\lambda_{\text{ex}} = 350$ nm. (b) CIE chromaticity diagram of the ratiometric oxygen sensing with Pt-2. (c) Pt-4, $\lambda_{\text{ex}} = 369$ nm. (d) CIE chromaticity diagram of the ratiometric oxygen sensing with Pt-3. The CIE data are derived from the emission spectra under different O₂ partial pressures.



Signal 1: VWD1 A, Wavelength=390 nm

Peak #	RetTime [min]	Type	Width [min]	Area mAU*s	Height [mAU]	Area %
1	3.403	PV	0.0561	1.25222	3.39819e-1	2.636e-3
2	5.843	PV	0.1443	5.40478	5.76751e-1	0.0114
3	11.740	PB	0.2898	4.74873e4	2535.85864	99.9621
4	15.620	BB	0.2797	11.36869	5.76275e-1	0.0239

Fig. S44 HPLC of Pt-1.



Peak #	RetTime [min]	Type	Width [min]	Area mAU*s	Height [mAU]	Area %
1	3.147	MM	0.0735	1.39858e4	3169.37280	98.7807
2	3.511	MM	0.0944	172.63608	30.49327	1.2193

Signal 1: VWD1 A, Wavelength=336 nm

Fig. S45 HPLC of Pt-2.

End of the supporting information.